Supplementary Information

Global ocean wave fields show consistent regional trends between 1980 and 2014 in a multi-product ensemble

1. Supplementary Notes 1: Description of global wave data products used

All products, except the visual observations, include assimilation of various sourced wind data. A graphical timeline of the assimilation techniques and products is shown in Supplementary Figure S1.

1.1 Global ocean wave reanalysis (coupled and with wave data assimilation)

The ECMWF research centre has released several ocean wave reanalysis products. Relevant to our analysis are ECMWF-ERAI and its succeeding ECMWF-ERA5 which are both briefly described below.

ECMWF-ERAI: Dee et al.[SM1] (hereafter ECMWF-ERAI) created a fourth generation of ECMWF atmospheric reanalysis by combining model data with historical observations. The ECMWF-ERAI was produced using a 4D-VAR data assimilation system as part of ECMWF Integrated Forecasting System (IFS) CY31R2 and simulates 6-hourly atmospheric fields at 0.70° spatial resolution from 1979-2019. The ocean wave parameters are available 6-hourly at 1.5° spatial resolution and are derived from a fully coupled atmosphere-wave model (ecWAM) that describes the evolution of ocean wave spectra, with assimilated satellite altimeter-retrieved wave height data (from 1991-onwards) to adjust the model-simulated wave spectra based on assumptions about contributions of wind-sea and swells. The ECMWF-ERAI assimilates along track data from satellite missions ERS-1, ERS-2, ENVISAT, JASON-1 and JASON-2, calibrated against offshore buoy data prior to assimilation. The ECMWF-ERAI wave data have been compared against both satellite altimetry and wave buoy observations[SM2, SM3]. As documented by Aarnes et al.[SM3], there is a potential for spurious trends in ECMWF-ERAI wave data when computed across a period extending from before and to after using altimeter data (~1992).

ECMFW-ERA5: Hersbach et al.[SM4] (hereafter ECMWF-ERA5) developed the fifth generation of ECMWF global atmospheric reanalysis which combines model data with vast amounts of past re-processed observations from across the world into a globally complete and consistent dataset. The ECMWF-ERA5 (reanalysis) was created using a 4D-VAR sophisticated data assimilation method as part of the new ECMWF Integrated Forecasting System (IFS) CY41R2 and simulates hourly atmospheric fields at 0.25° spatial resolution from 1979-onwards. The ocean wave parameters are also derived from a fully coupled atmosphere-ocean-wave model (ecWAM), which assimilates satellite radar altimeter-derived wave height data from 1991-present. The assimilation is based a simple optimum interpolation scheme adapted to run as part of ECMWF IFS. In addition to

assimilating along track data from ERS-1, ERS-2, ENVISAT, JASON-1, and JASON-2, ECMWF-ERA5 also assimilates wave height data from CRYOSAT-2 and SARAL. All data were calibrated against ECMWF global model data prior to assimilation. The calibrations against ECMWF global model data have sharply reduced potentially spurious trends. It is, nevertheless, a limitation of using altimeter wave height within global reanalysis as no global wave data were available before a certain time. The ecWAM wave model is based on wind-wave growth parameterizations of WAM cycle 4 (commonly known as ST3)[SM4]. The ECMWF-ERA5 ocean wave reanalysis comprises various enhancements over its previous ECMWF versions, with hourly model outputs available at 0.5° resolution. The ECMWF-ERA5 ocean wave parameters have been compared against satellite altimeter measurements and buoy observations[SM5].

1.2 Global ocean wave hindcasts (uncoupled and without wave data assimilation)

Global wave hindcasts (with sea-ice forcing)

ECMWF-ERA5H: Bidlot et al.[SM5] (hereafter ECMWF-ERA5H) produced a global wave hindcast by forcing ecWAM (standalone) CY46R1 with hourly 10m neutral winds and daily sea-ice concentrations from ECMWF ERA5 atmospheric reanalysis. The ecWAM model was implemented at 0.125° spatial resolution, with spectral ordinates discretized across 36 frequencies and 36 directions. The model settings included ST4 source-term physics. The details of its implementation in ecWAM, are however, slightly different as explained in the ECMWF IFS documentation[SM6]. The bathymetry of ECMWF-ERA5H is represented by ETOPO1, and wave model outputs are available hourly at 0.25° spatial resolution. The ECMWF-ERA5H ocean wave parameters have been compared against both satellite altimeter measurements and buoy observations[SM5].

KU-JRA55: Mori et al.[SM7] and Shimura et al. [SM8] (hereafter KU-JRA55) developed a global ocean wave hindcast by driving WW3 wave model version 3.14 with 6-hourly surfaces and monthly sea-ice forcing from JRA55 atmospheric reanalysis. The wave model was implemented using default ST2 source-term physics with the wave spectra discretized over 29 frequencies and 30 directions. The model domain consists of a global grid at 0.56° resolution and model outputs are archived at 1-hourly intervals.

IORAS-MERRA2: Sharmar et al.[SM9] (hereafter IORAS-MERRA2) produced a global wind-wave hindcast by forcing WW3 wave model version 4.14 with 6-hourly surface wind fields and hourly sea-ice concentration fields from NASA MERRA-2 atmospheric reanalysis. The WW3 model was implemented using ST4 source-term physics with default settings, with model outputs archived on a global grid with ~0.5° x 0.625° at 6-hourly intervals. The IORAS-MERRA2 wave hindcast has been compared against other wave hindcasts as well as visual observations and satellite altimeter data [SM9].

NOC-ERAI: Bricheno and Wolf[SM10] (hereafter NOC-ERAI) created a global wave hindcast using WW3 wave model version 3.14 forced by 6-hourly surface winds and daily sea-ice concentration

fields from ECMWF ERA-Interim atmospheric reanalysis. The WW3 model was setup using ST2 source-term physics with wave spectra discretized across 30 frequencies and 36 directions. The spatial resolution was set at ~0.7° x 0.5° with wave model outputs available at 1-hourly intervals.

IHC-GOW1.0: Reguero et al.[SM11] created Global Ocean Waves (GOW) wave hindcast by forcing WW3 wave model version 2.22 with 6-hourly surface wind fields obtained from the NCEP/NCAR atmospheric reanalysis and hourly sea-ice forcing from NCAR coupled MOM3 sea-ice model. The model was implemented using default ST2 source-term physics, with the wave spectra discretized over 25 frequencies and 72 directions. The WW3 model uses a global grid with 1.5° x 1.0° spatial resolution and wave model outputs are available at hourly intervals. IHC-GOW1.0 has undergone a series of calibration/validation procedures against significant wave height measurements derived from satellite altimeters and buoy instruments [SM11].

CFSR-driven wave hindcasts (with sea-ice forcing)

IHC-GOW2.0: Perez et al.[SM12] (hereafter IHC-GOW2.0) created an updated hindcast of GOW1.0 driven by 1-hourly surface winds from the CFSR atmospheric reanalysis and hourly sea-ice forcing from the CFSR coupled MOM4 sea-ice model. The IHC-GOW2.0 is based on WW3 model version 4.18 and uses default ST4 source-term physics. The wave model was implemented on a multi-grid scheme with a series of "two-way" nested domains covering oceanic basins at 0.5° resolution and continental shelf regions at 0.25° resolution. The wave spectra are discretized over 32 frequencies and 24 directions with model outputs available at hourly intervals. The WW3 model data has been validated against wave spectral information from multiple surface buoy stations and multi-mission satellite altimeter measurements[SM12].

CSIRO-CAWCR: Durrant et al.[SM13] and Smith et al.[SM14] (hereafter CSIRO-CAWCR) developed a global wave hindcast using versions 4.08 and v4.18 of WW3. The atmospheric forcing of the wave model were hourly surface winds obtained from CFSR reanalysis between 1979-2014. Sea-ice concentrations fields at hourly intervals from CFSR´s coupled MOM4 sea-ice model were used. The model was implemented at 0.4° resolution using ST3 source-term package with βmax adjusted to 1.33. The wave model spectra are discretized over 29 frequencies and 24 directions with wave model outputs available at 1-hourly resolution.

IFREMER-CFSR: Stopa et al.[SM15] (hereafter IFREMER-CFSR) produced a global wave hindcast by forcing WW3 wave model version 5.16 with satellite-corrected hourly surface wind fields from CFSR reanalysis and hourly sea-ice forcing fields from CFSR coupled MOM4 sea-ice model. Parameterizations of wave generation and dissipation proposed by Ardhuin et al. [SM16] and the non-linear Discrete Interaction Approximation by Hasselman[17]. It has been shown that this model configuration works well for sea and swell partitions in comparison to other parameterization packages[SM18]. The global model is implemented at latitude and longitude grid of 0.5º with a spectral bin composed of 24 directions and 32 frequencies that are exponentially spaced from 0.037 to 0.7Hz at an increment of 10%. The wind and ice fields at spatial resolution of 0.2º (22 km) from the Climate Forecast System Reanalysis (CFSR) [SM19,20] are used to force the model runs. The hindcast was calibrated and corrected in time to match a homogenized satellite

altimetry database of Queffeulou and Croizen-Fillon[SM15,21,22]. IFREMER-CFSR is calibrated in time to match the monthly hemispheric statistics computed from satellite altimetry H_s. The hindcast closely matches the trends of the satellite altimeter but instantaneously the hindcast is largely independent to co-locations of H_s satellite altimetry. The notable discrepancies in CFSR such as the step change in 1994[SM2,23,24] are mitigated using this method.

Global wave hindcasts without sea-ice forcing

JRC-ERAI: Mentaschi et al.[SM25] (hereafter JRC-ERAI) created a global wave hindcast by forcing WW3 wave model version 4.08 with 6-hourly surface winds obtained from ECMWF ERA-Interim atmospheric reanalysis. The model was run without sea-ice concentration forcing fields using ST4 source-term physics, with default settings. The WW3 wave model was implemented at 1° spatial resolution with wave model outputs available at 12-hourly intervals.

JRC-CFSR: Mentaschi et al. [SM25] (hereafter JRC-CFSR) created a global wave hindcast by forcing WW3 wave model version 4.08 with surface wind fields from CFSR atmospheric reanalysis. The WW3 model was implemented without sea-ice forcing fields. The WW3 setup uses ST4 source-term physics the wind-wave growth parameter (β_{max}) adjusted to 1.52. The WW3 model domain consists of a global grid at 1.5° spatial resolution, with nested subgrids setup across specific regions at 0.25 and 0.5° spatial resolutions. Model outputs are available at 3-hourly resolution. JRC-CFSR has been compared against multi-mission satellite-retrieved measurements, buoy observations and JRC-ERAI[SM25].

1.3 Visual data (VOS)

IORAS-VOS: Annual and monthly estimates of ocean significant wave height and dominant wave periods contributed to IORAS were obtained from visual observation data by Voluntary Observing Ships (hereafter VOS) assimilated in ICOADS (International Comprehensive Ocean Atmosphere Data Set)[SM26]. Quality control data procedures, ad-hoc corrections, pre-processing were applied to individual observations according to refs.[SM27-30]. Spatial gridding of VOS wave data is affected by inhomogeneous sampling, implying more than 500 observations per month per 2° grid cell across well sampled areas and less than 5 observations across poorly sampled areas (e.g., Southern Ocean). Therefore, gridding was provided by averaging all available wave data for sampled grid cells with at least 10 observations for calendar month.

1.4 Satellite data (IMOS and ECCI)

IMOS: Ribal and Young [SM31] (hereafter IMOS) assembled a satellite wave dataset using data from 13 altimeters from 1985-present. The along track data from satellite GEOSAT, ERS-1, TOPEX, ERS-2, GFO, and ENVISAT were derived from GLOBWAVE online archive. The raw data from more recent missions of JASON-1, JASON-2, CRYOSAT-2, SARAL, JASON-3 as well as SENTINEL-3A were derived from RADS online archive. The raw data for HY-2A was obtained from National Satellite Ocean Application Service of China (NSOAS). Each satellite mission was

independently calibrated against NDBC buoy data, and subsequently validated against an independent buoy data and other altimeters. Particular care was taken to identify discontinuities or drift in calibrations over time and when detected, these were removed by piece-wise calibration[SM31].

ECCI: Dodet et al.[SM32] assembled a satellite wave dataset called "Sea State CCI dataset" (hereafter ECCI) which inherits from GLOBAWAVE´s database project building on experience and existing outputs. ECCI extends and enhances GLOBWAVE products, which were a post-processing across existing L2 altimeter agency products with additional filtering, corrections, and variables and spans years 1992 through 2018[SM32]. In our analysis, merged daily products retaining all valid and good quality measurements from all altimeters across single days were used to aggregate and compute seasonal statistics. In GLOBWAVE, calibration methods were developed and applied to data from ERS-1, TOPEX, ERS-2, GFO, JASON-1, ENVISAT, and JASON-2 to account for changes within Geophysical Data Records (GDR) provided by government space agencies. Most satellite missions were linearly calibrated against buoy measurements from United States (National Buoy Center), Canada (Environment Canada), and Europe (Meteo-France, UKMet Office, and Spanish Puerto del Estado). One exception is TOPEX for which data during the drifting period (1996–1999) were also corrected using crossovers with ERS-2 or GFO. JASON-1, JASON-3, CRYOSAT-2, and SARAL all operated at the same time as JASON-2. For these missions, JASON-2 was taken as the reference and each of these missions was calibrated against JASON-2 at cross-over points.

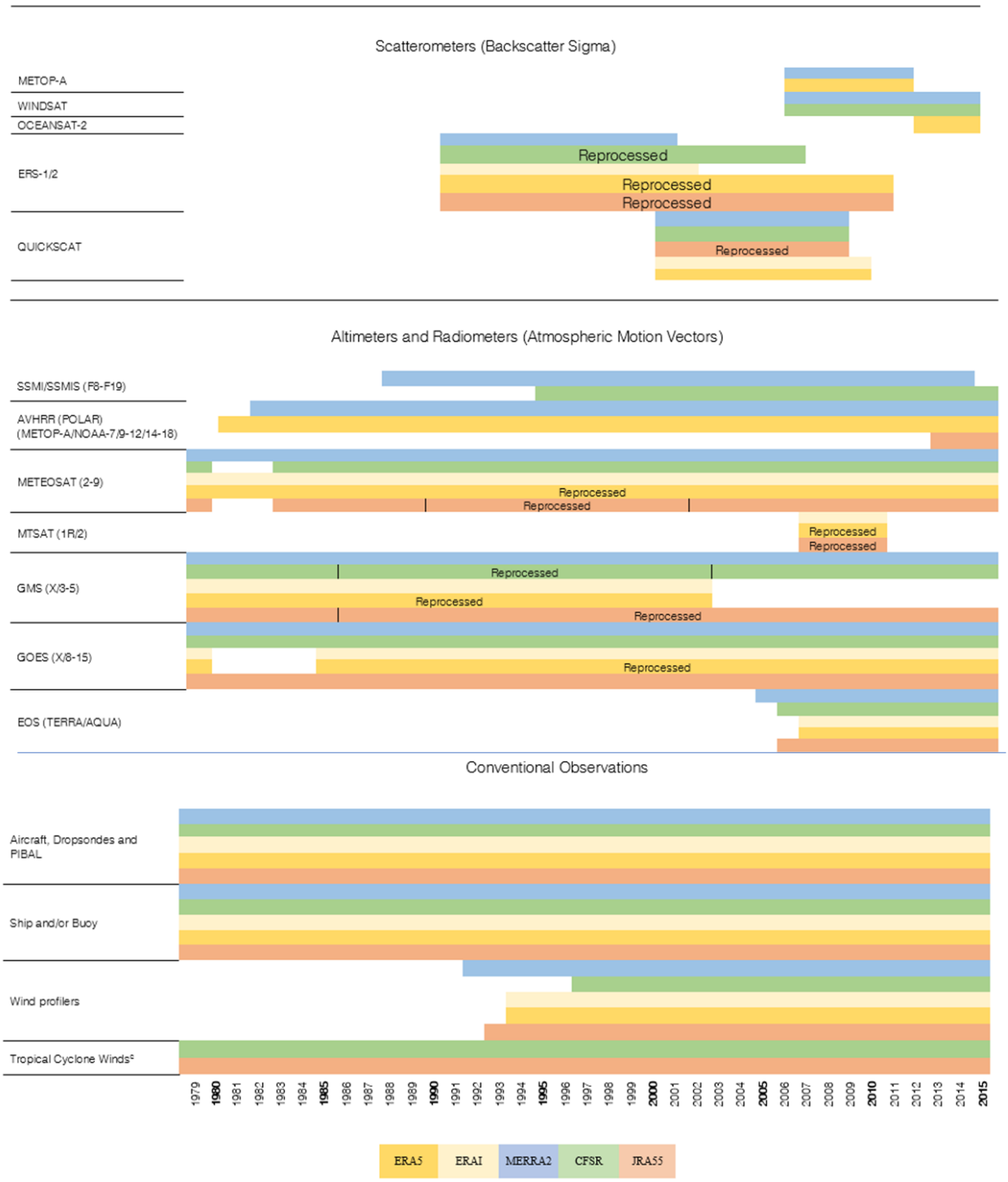

Supplementary Figure S1. Timeline of wind data assimilation for the different wind reanalysis products. Years are full years and lines represent reprocessed data.

2. Supplementary Notes 2: Climatological means of seasonal wave characteristics

Prior to calculating trends, the seasonal wave climatology represented by each wave data product was evaluated. Qualitative comparison of time-averaged seasonal significant wave height (H_s) across all products exhibit expected alternating patterns of higher H_s across Northern and Southern Hemispheres for DJF and JJA seasons, respectively (Supplementary Figure S2). Globally averaged DJF H_s^{50} and H_s^{90} across all model and reanalysis members (1-12; Table 1) are 2.24 m ± 1.01 m and 3.19 m ± 1.46 m respectively, 5 and 11% lower than respective globally averaged primary IMOS altimeter reference dataset. The error values represent plus/minus one standard deviation as computed across all spatial grid cells. The JJA season exhibits a similar behavior, with the 12-member globally averaged ensemble being 6% and 14% lower compared to the satellite reference data (Supplementary Table S1).

Whilst the different products and ensemble patterns are within expectations and in qualitative agreement with satellite-based patterns, variability amongst models is rather large, exceeding 1 m for H_s^{90} in high-energy regions of the North Pacific, Atlantic and Southern Oceans (Supplementary Figures S2A-C and S3A-C). To better quantify inter-model variability, we compare annual values in DJF/JJA of each ensemble member against our chosen satellite reference data using three skill measures: bias, unbiased root-mean-square difference (*urmsd*), and an index of agreement (*IoA*); *bias* and *urmsd* values are sought to be low, while a larger *IoA* near 1 indicates good skill. *Bias* and *urmsd* are defined in the Methods Section. *IoA* is calculated as[SM33]:

$$IoA = \frac{1 - \sum_{i=1}^{N} \left| s_{mdl}^{i} - s_{sat}^{i} \right|^2}{\sum_{i=1}^{N} \left(\left| s_{mdl}^{i} - \bar{s}_{mdl} \right| + \left| s_{sat}^{i} - \bar{s}_{sat} \right| \right)^2}$$

where s is the variable in question (H_s in this case), mdl is the sea state product (hindcast, reanalysis, or observation), sat is the satellite derived altimeter data, and N the total number of observations. Overall, climatological (temporally averaged seasonal H_s) skill statistics are superior for H_s^{50} DJF and JJA compared to H_s^{90} . Climatology biases between individual models and satellite data are ± 0.35 m for H_s^{50} DJF and JJA but approach 1.5 m with nearly a 2 m range (from -0.50 m to +1.40 m) for H_s^{90} (Supplementary Table S2). Similarly, H_s^{50} *urmsd* and *IOA* are better compared to H_s^{90}. Close inspection of the individual products show a marked difference between the skill scores of the first 7 products compared to the remaining ones as was also found with the trends and discussed in *Methods, Ensemble Selection*. Also of note, is that the skill scores of the VOS dataset are substantially worse compared to the dynamically modeled products; this is attributed to the lack of VOS data in the southern hemisphere (Supplementary Figures S1B and S2B) leading to greater weighting of the skill assessment to the northern hemisphere compared to the other sea-state products.

Supplementary Table S1. Globally averaged significant wave height statistics (1985-2014).

	DJF		JJA	
	p50 mean	**p90 mean**	**p50 mean**	**p90 mean**
12-member ensemble*	2.24 ± 1.01	3.19 ± 1.46	2.21 ± 1.24	3.00 ± 1.74
7-member ensemble*	2.35 ± 0.88	3.74 ± 1.50	2.41 ± 1.17	3.60 ± 1.81
VOS	2.60 ± 0.91	4.21 ± 1.48	2.77 ± 0.91	4.49 ± 1.49
IMOS altimeter	2.35 ± 1.18	3.60 ± 1.38	2.35 ± 1.18	3.48 ± 1.67

** Mean and standard deviations are calculated across all grid cells (0.5° x 0.5° resolution) on the 12 and 7- member ensemble averaged climatology maps. Variance across the 12 and 7 members are shown in Supplementary Figures S3C and S3C.*

Supplementary Table S2. Skill statistics comparing climatologically averaged (1985-2014) H_s on a per grid cell basis between contributed sea-state products and the altimeter reference dataset IMOS.

	H_s^{50} DJF			H_s^{50} JJA			H_s^{50} JJA			H_s^{90} JJA		
Product	***bias***	***urmsd***	***IOA***	***bias***	***urmsd***	***IOA***	***bias***	***urmsd***	***IOA***	***bias***	***urmsd***	***IOA***
ECMWF-ERA5	-0.09	0.10	0.99	-0.10	0.09	1.00	-0.24	0.16	0.99	-0.24	0.13	0.99
ECMWF-ERAI	-0.02	0.62	0.82	-0.07	0.43	0.91	-0.22	0.19	0.99	-0.23	0.15	0.99
ECMWF-ERA5H	-0.05	0.12	0.99	-0.05	0.10	1.00	-0.12	0.21	0.99	-0.10	0.16	1.00
KU-JRA55	0.14	0.23	0.97	0.10	0.20	0.99	0.23	0.35	0.97	0.17	0.27	0.98
IORAS-MERRA2	-0.31	0.17	0.95	-0.32	0.12	0.98	-0.48	0.24	0.96	-0.45	0.19	0.98
NOC-ERAI	0.08	0.22	0.98	0.08	0.12	0.99	1.45	0.53	0.79	1.38	0.41	0.85
IHC-GOW1.0	0.04	0.21	0.98	0.00	0.17	0.99	0.00	0.31	0.99	-0.04	0.23	0.99
IHC-GOW2.0	0.00	0.18	0.99	0.01	0.54	0.94	-0.05	0.32	0.98	-0.03	0.74	0.95
CSIRO-CAWCR	0.06	1.08	0.61	0.01	0.79	0.67	0.03	0.39	0.98	0.09	0.24	0.99
IFREMER-CFSR	-0.07	0.33	0.96	-0.17	0.58	0.93	-0.09	0.37	0.98	-0.16	0.56	0.97
JRC-CFSR	0.08	0.31	0.97	0.14	0.29	0.98	0.04	0.40	0.98	0.15	0.46	0.98
JRC-ERAI	0.02	0.31	0.97	0.08	0.31	0.98	-0.07	0.43	0.97	0.05	0.53	0.97
VOS	0.26	0.38	0.94	0.39	0.40	0.76	0.67	0.56	0.92	0.83	0.53	0.71
Ensemble means												
12-member	-0.05	0.37	0.95	-0.05	0.44	0.95	0.03	0.45	0.97	0.02	0.58	0.97
7-member	-0.04	0.23	0.98	-0.06	0.16	0.99	0.10	0.33	0.98	0.07	0.25	0.99

Highlighted green entries indicate good agreement based on thresholds: $bias \leq |0.10|m$*; urmsd ≤= 0.25m; IOA ≥ 0.97.*

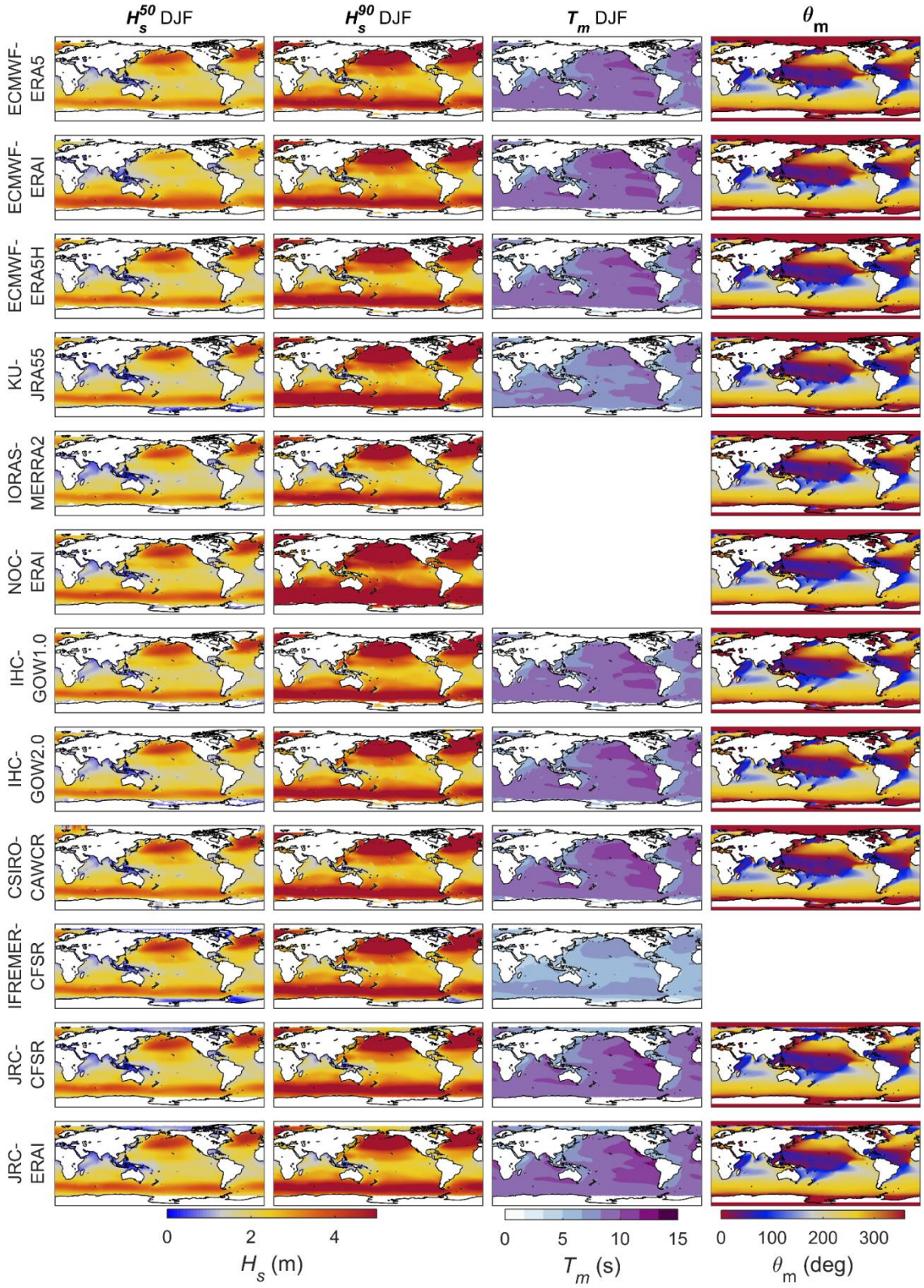

Supplementary Figure S2A. Climatological mean of median (H_s^{50}) and 90th percentile (H_s^{90}) significant wave heights, mean wave periods (T_m) and mean wave directions (θ_m) for the DJF

season. Climatological means are calculated over the time-period of the IMOS dataset, 1985 through 2014 (30 years).

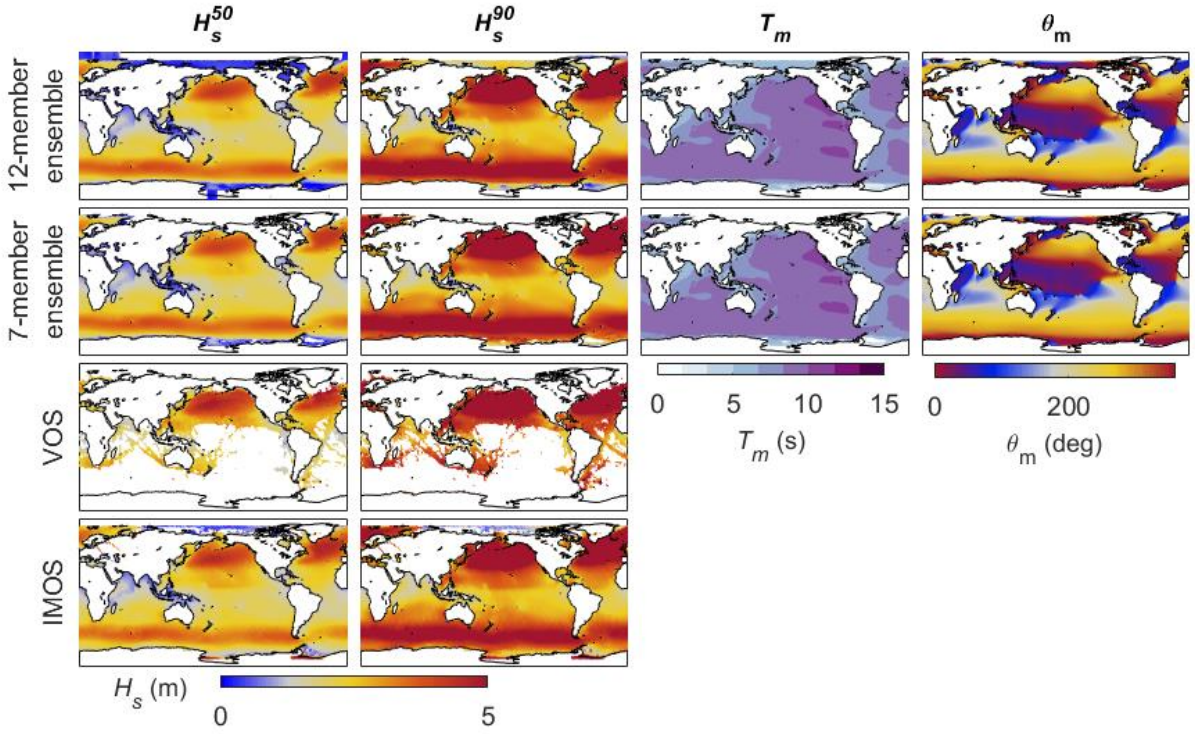

Supplementary Figure S2B. Ensemble climatological means of the median (H_s^{50}) and 90th percentile (H_s^{90}) significant wave heights, mean wave periods (T_m) and mean wave directions (θ_m) for the DJF season. Ensemble means are shown for the first 12 and 7 sea state products listed in Table 1 and compared to ship-based observations (VOS), and the IMOS altimeter reference dataset.

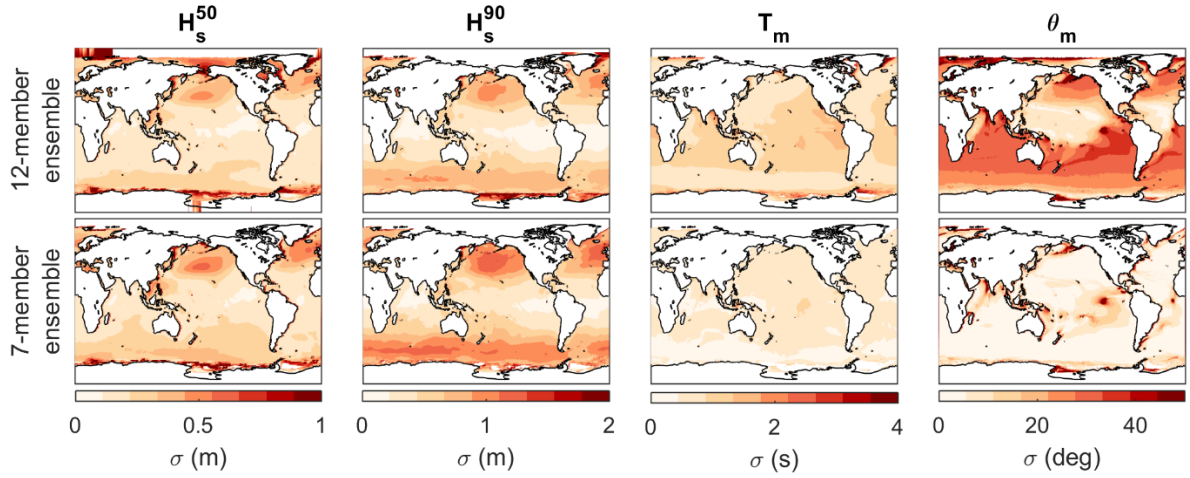

Supplementary Figure S2C. Spatial variance of the 12- and 7-member ensemble means.

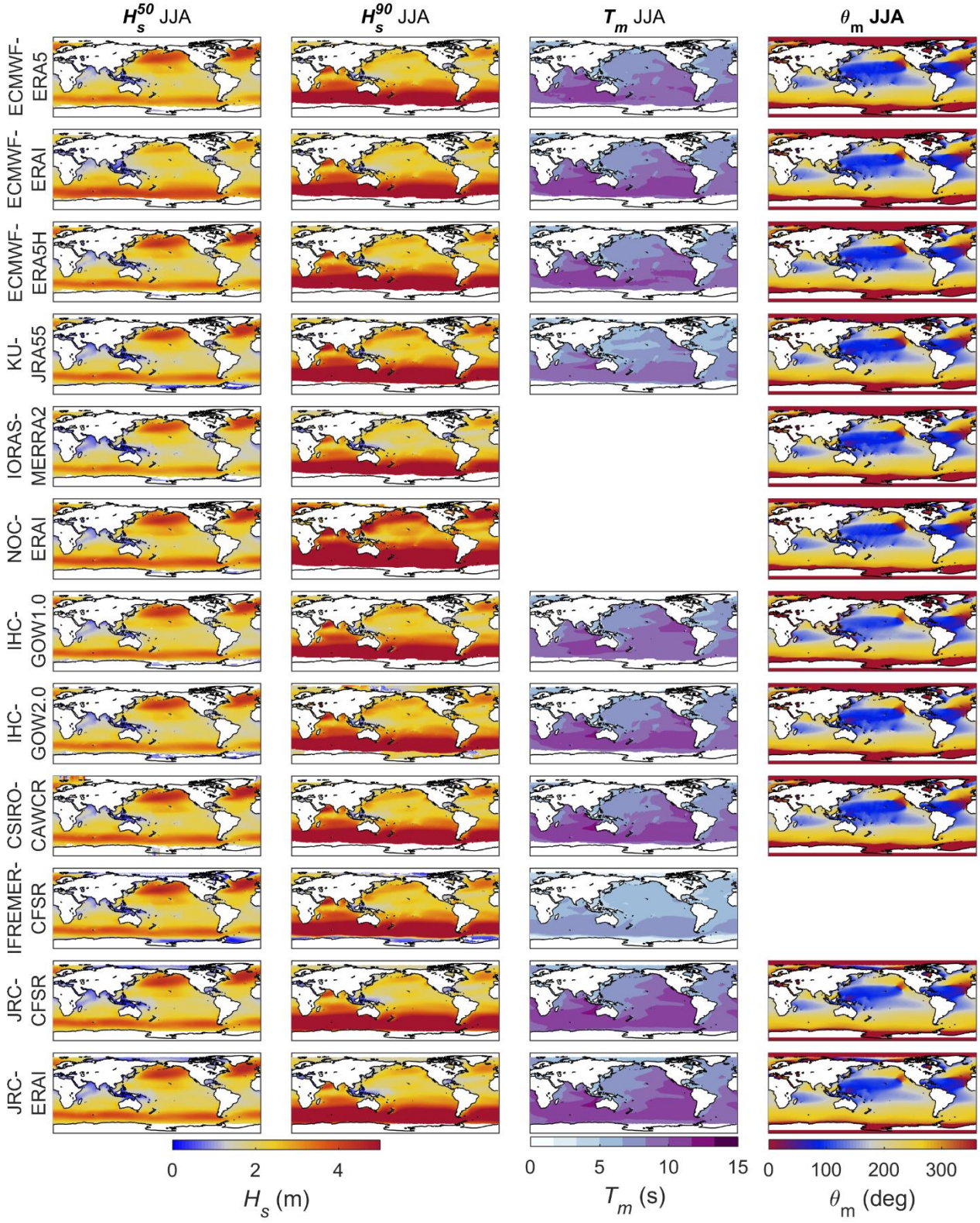

Supplementary Figure S3A. Climatological mean of median (H_s^{50}) and 90th percentile (H_s^{90}) significant wave heights, median mean wave period (T_m) and median mean directions (θ_m) for the JJA season. Climatological means are calculated over the time-period of the IMOS dataset, 1985 through 2014 (30 years).

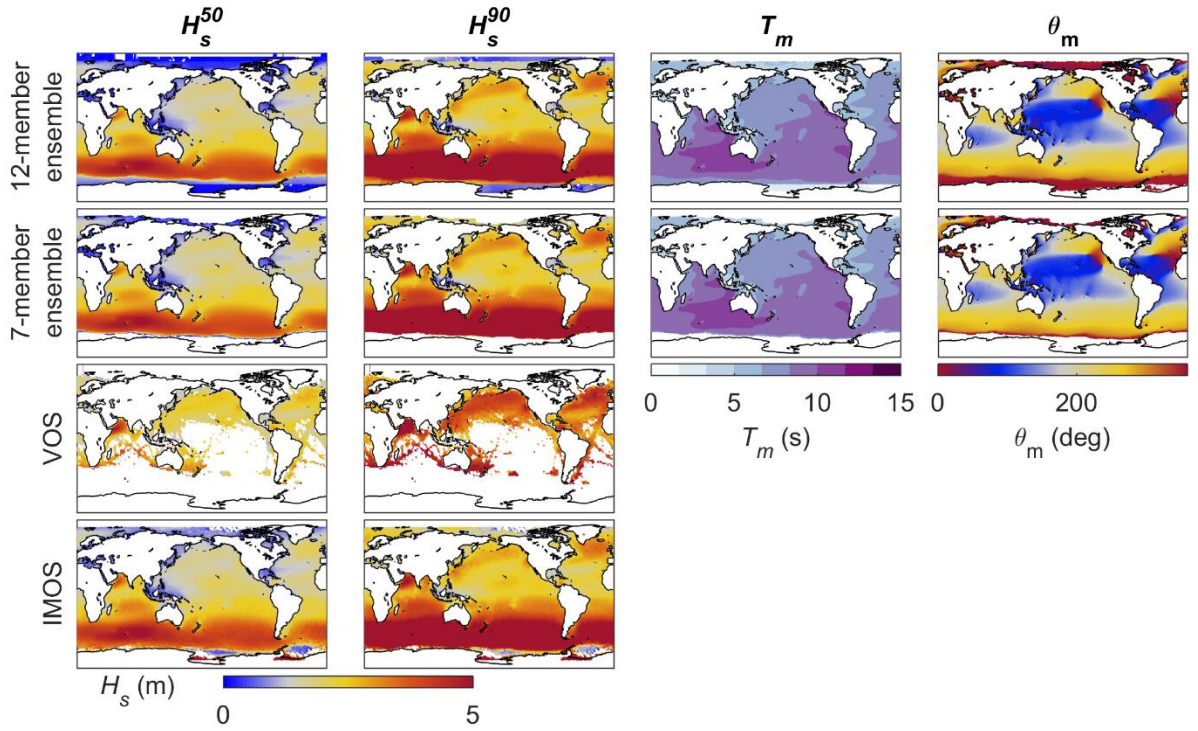

Supplementary Figure S3B. Same as in Supplementary Figure S2B but for the JJA season.

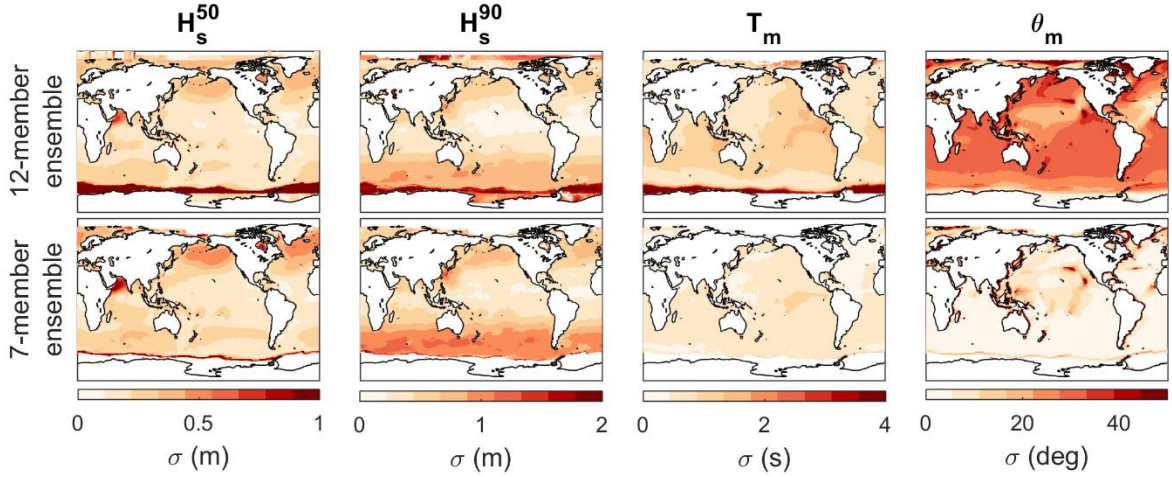

Supplementary Figure S3C. Same as in Supplementary Figure S2C but for the JJA season.

3. Supplementary Notes 3: Trend maps of all contributed wave state products

In this Section, trend maps of individual contributed wave state products and the 7-member and 12-member ensembles are shown for the two time-periods corresponding to altimeter datasets IMOS (RY19) (1985-2014) and ECCI (1995-2014).

Additionally, we present here histograms of all trend values from the 7-member ensemble over the period 1980-2014 (Supplementary Fig. S6). The histograms show the full range and the 5^{th} and 95^{th} percentiles of computed trend values for each of the wave state variables.

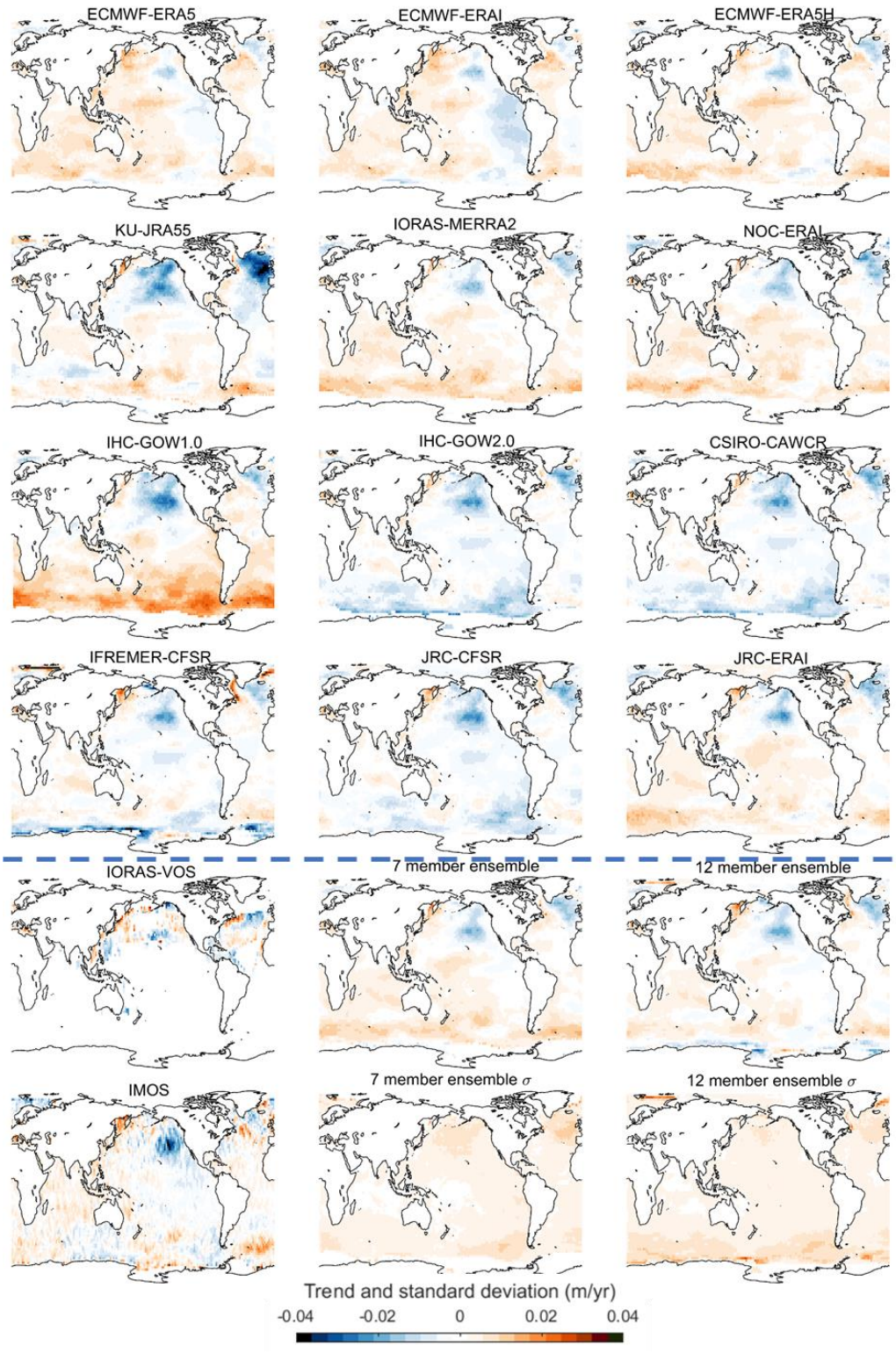

Supplementary Figure S4A. Trends (m/yr) in DJF median significant wave heights (H_s^{50}) for the 1985-2014 period that is commensurate with the IMOS altimeter reference dataset. The 7-member ensemble σ show the ensemble mean and standard deviation of the

first 7 members. The 12-member ensemble is for all members except the VOS which are excluded due to data sparsity.

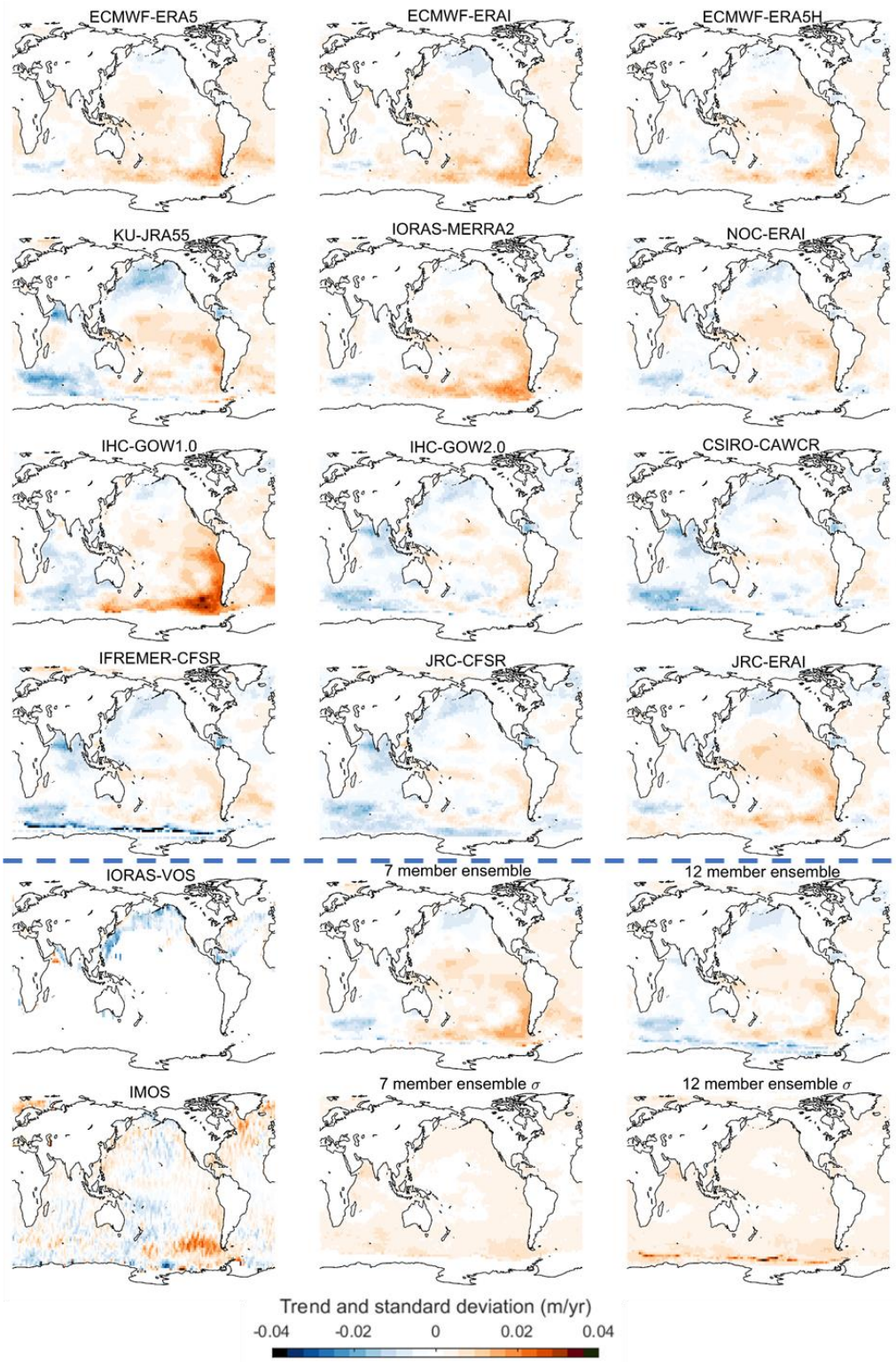

Supplementary Figure S4B. Trends (m/yr) in JJA median significant wave heights (H_s^{50}) for the 1985-2014 period that is commensurate with the IMOS altimeter reference dataset. The 7-member ensemble σ show the ensemble mean and standard deviation of the first 7 members. The 12-member ensemble is for all members except the VOS which are excluded due to data sparsity.

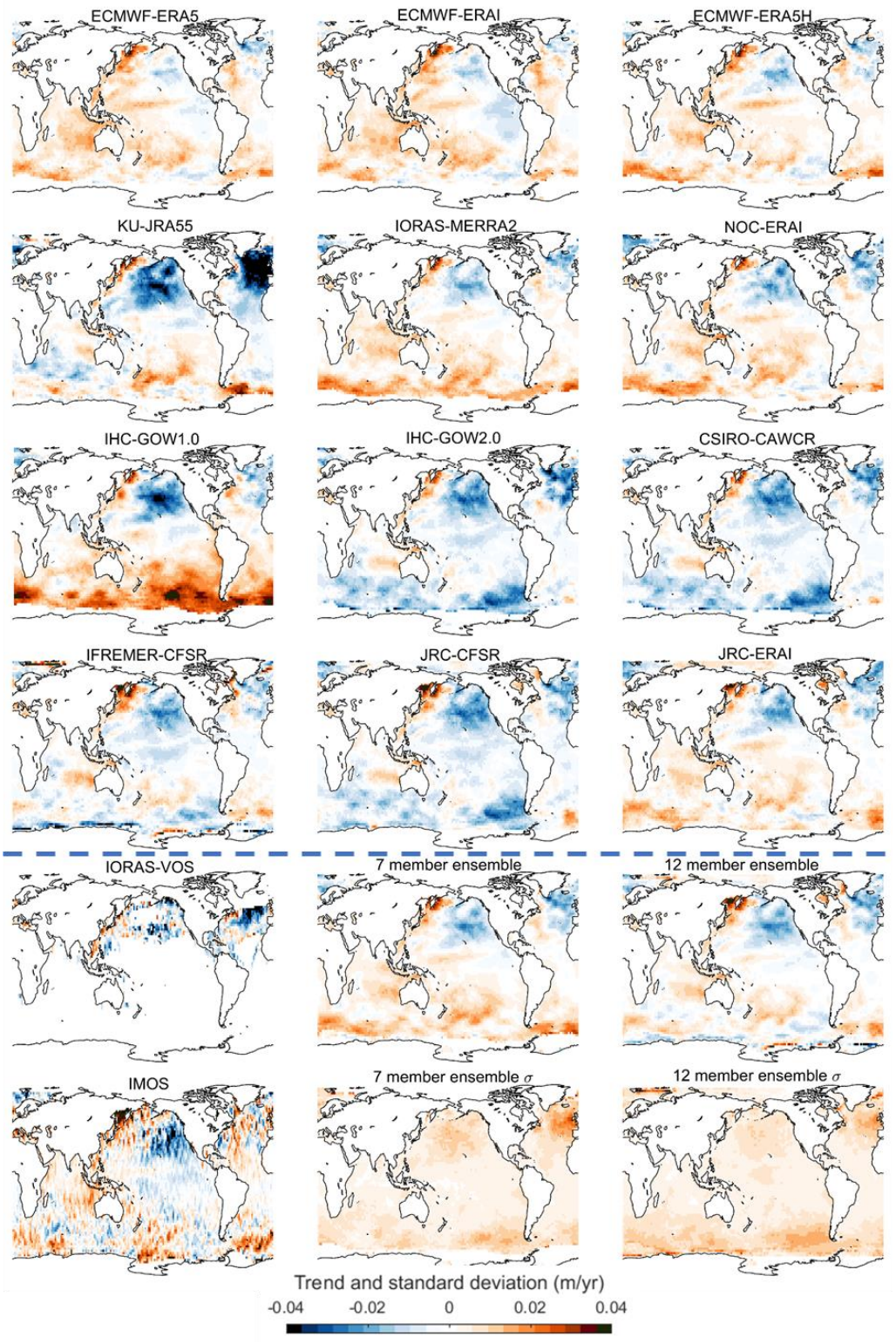

Supplementary Figure S4C. Trends (m/yr) in DJF 90th percentile significant wave heights (H_s^{90}) for the 1985-2014 period that is commensurate with the IMOS altimeter reference dataset. The 7-member ensemble σ show the ensemble mean and

standard deviation of the first 7 members. The 12-member ensemble is for all members except the VOS which are excluded due to data sparsity.

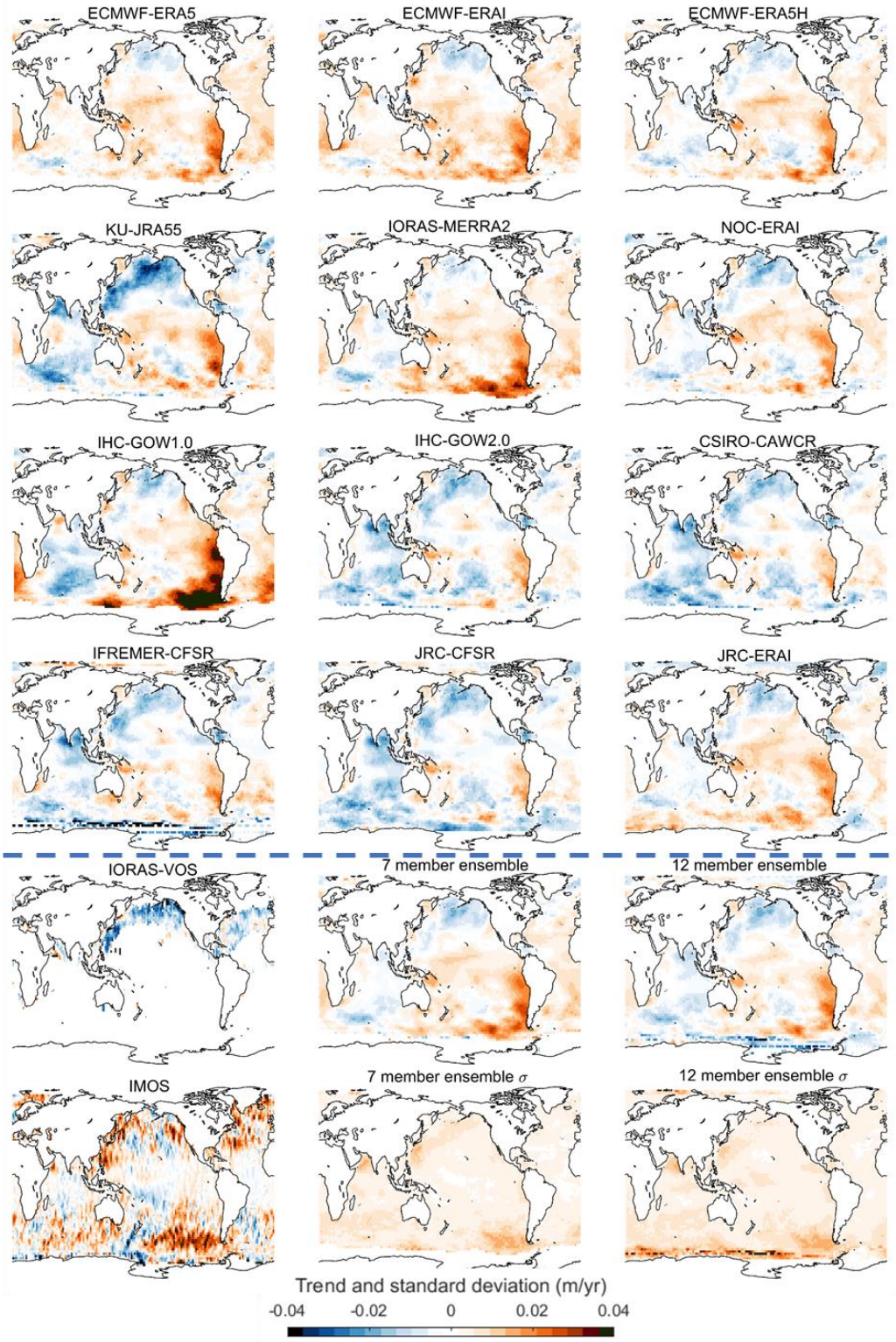

Supplementary Figure S4D. Trends (m/yr) in JJA 90th percentile significant wave heights (H_s^{90}) for the 1985-2014 period that is commensurate with the IMOS altimeter reference dataset. The 7-member ensemble σ show the ensemble mean and standard deviation of the first 7 members. The 12-member ensemble is for all members except the VOS which are excluded due to data sparsity.

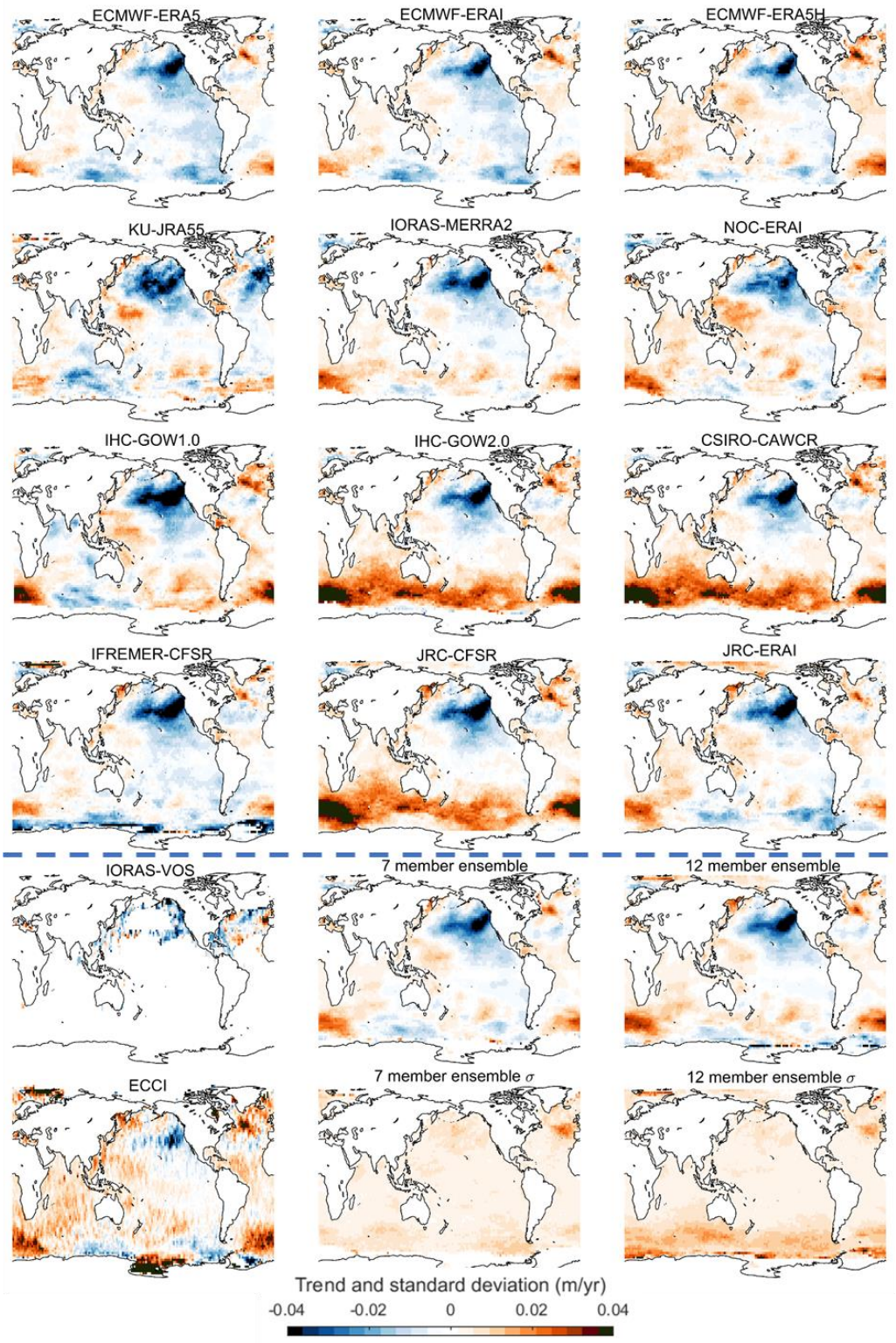

Supplementary Figure S5A. Same as in Supplementary Figure S4A (trends in DJF H_s^{50}) but for the 1995-2014 time-period that is commensurate with the ECCI altimeter reference dataset.

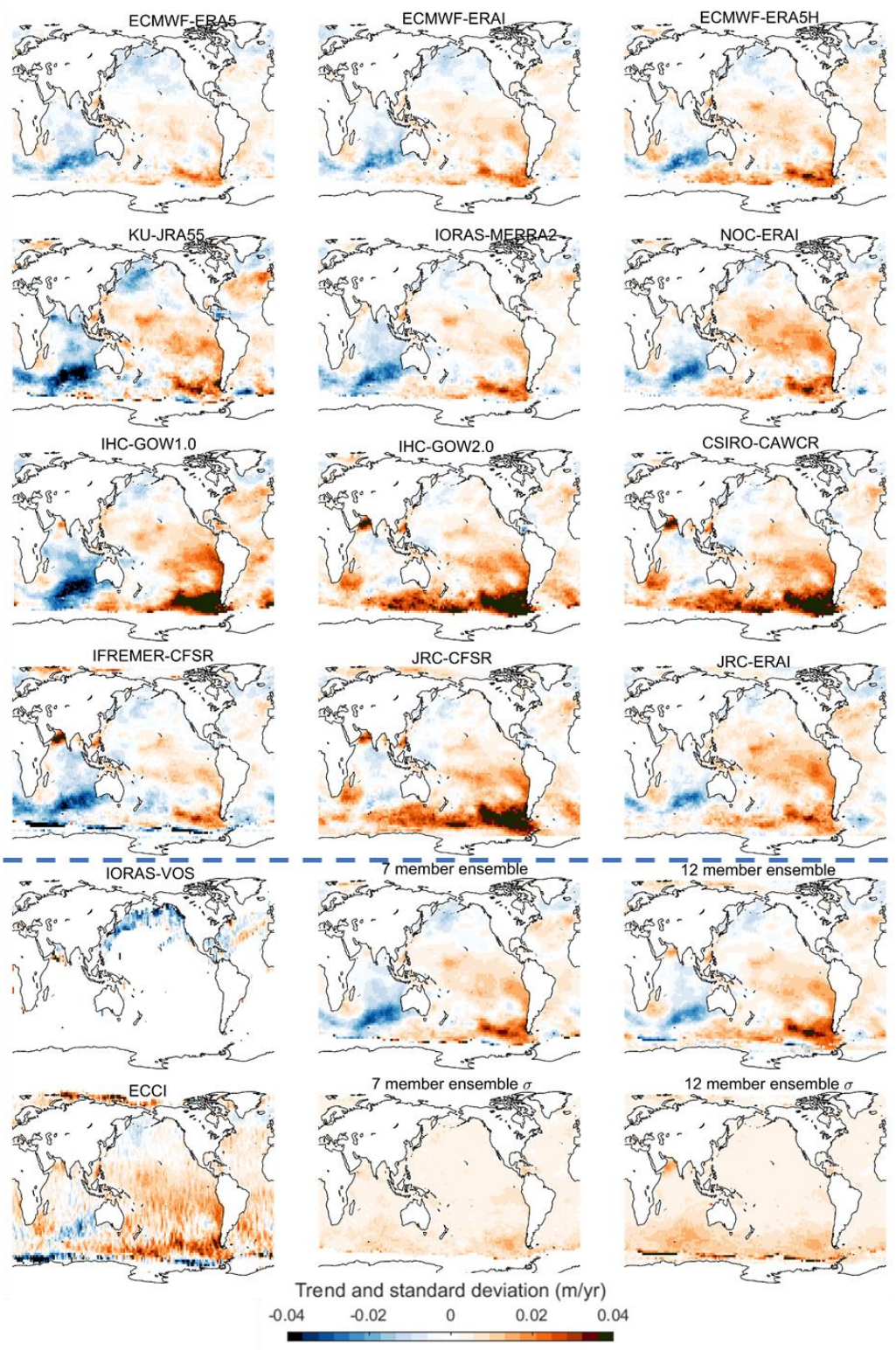

Supplementary Figure S5B. Same as in Supplementary Figure S4B (trends in JJF H_S^{50}) but for the 1995-2014 time-period that is commensurate with the ECCI altimeter reference dataset.

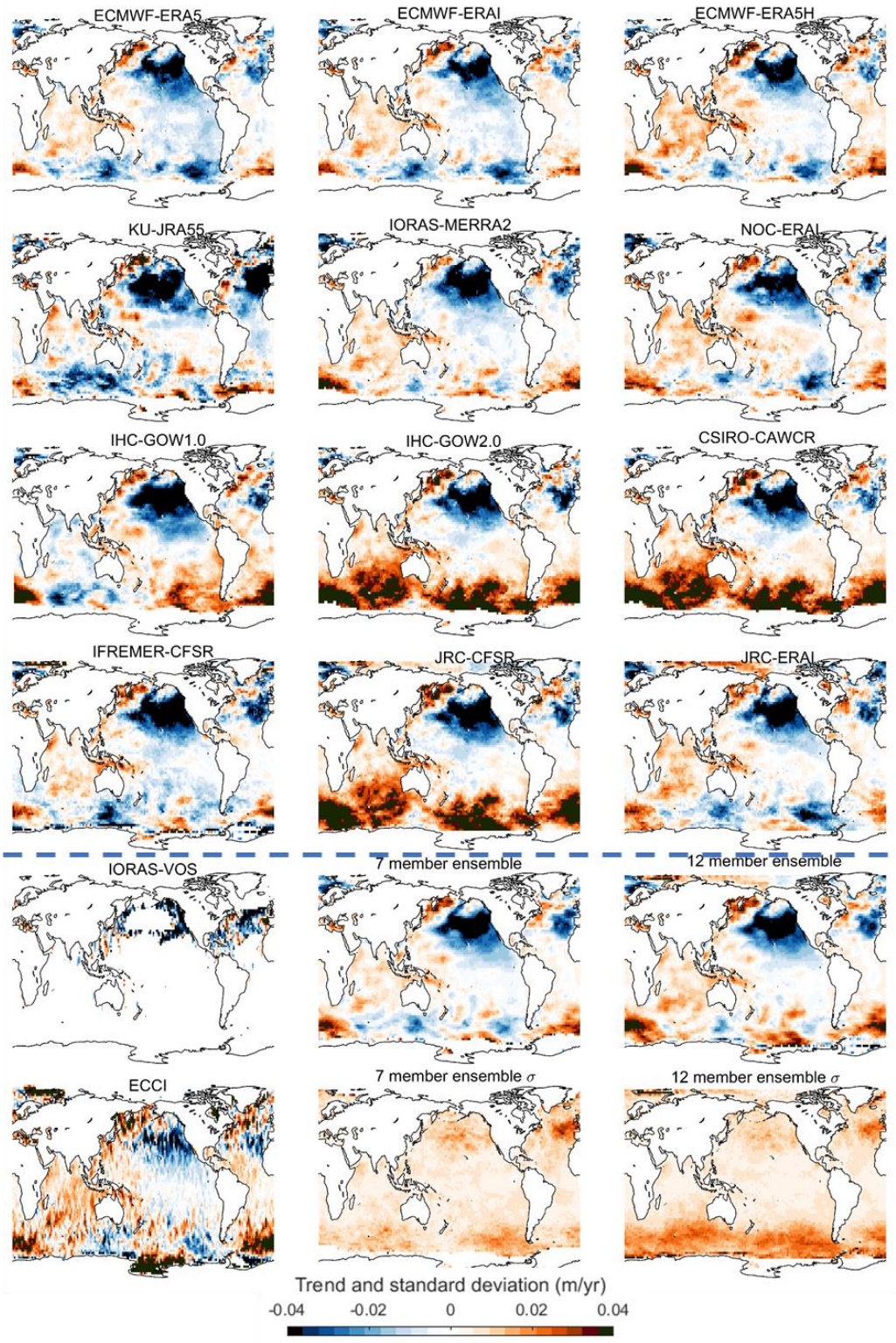

Supplementary Figure S5C. Same as in Supplementary Figure S4C (trends in DJF H_s^{90}) but for the 1995-2014 time-period that is commensurate with the ECCI altimeter reference dataset.

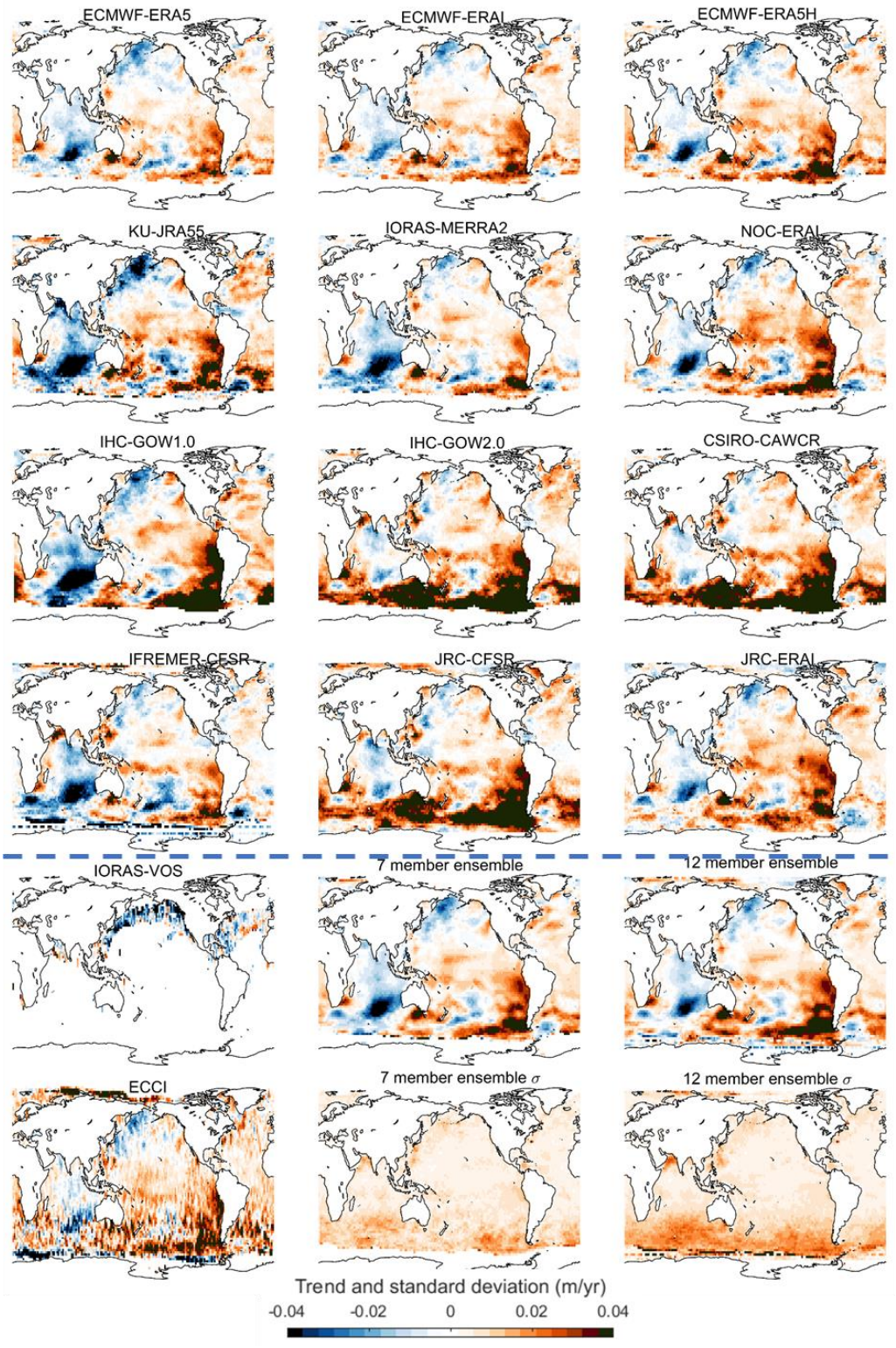

Supplementary Figure S5D. Same as in Supplementary Figure S4D (trends in JJA H_s^{90}) but for the 1995-2014 time-period that is commensurate with the ECCI altimeter reference dataset.

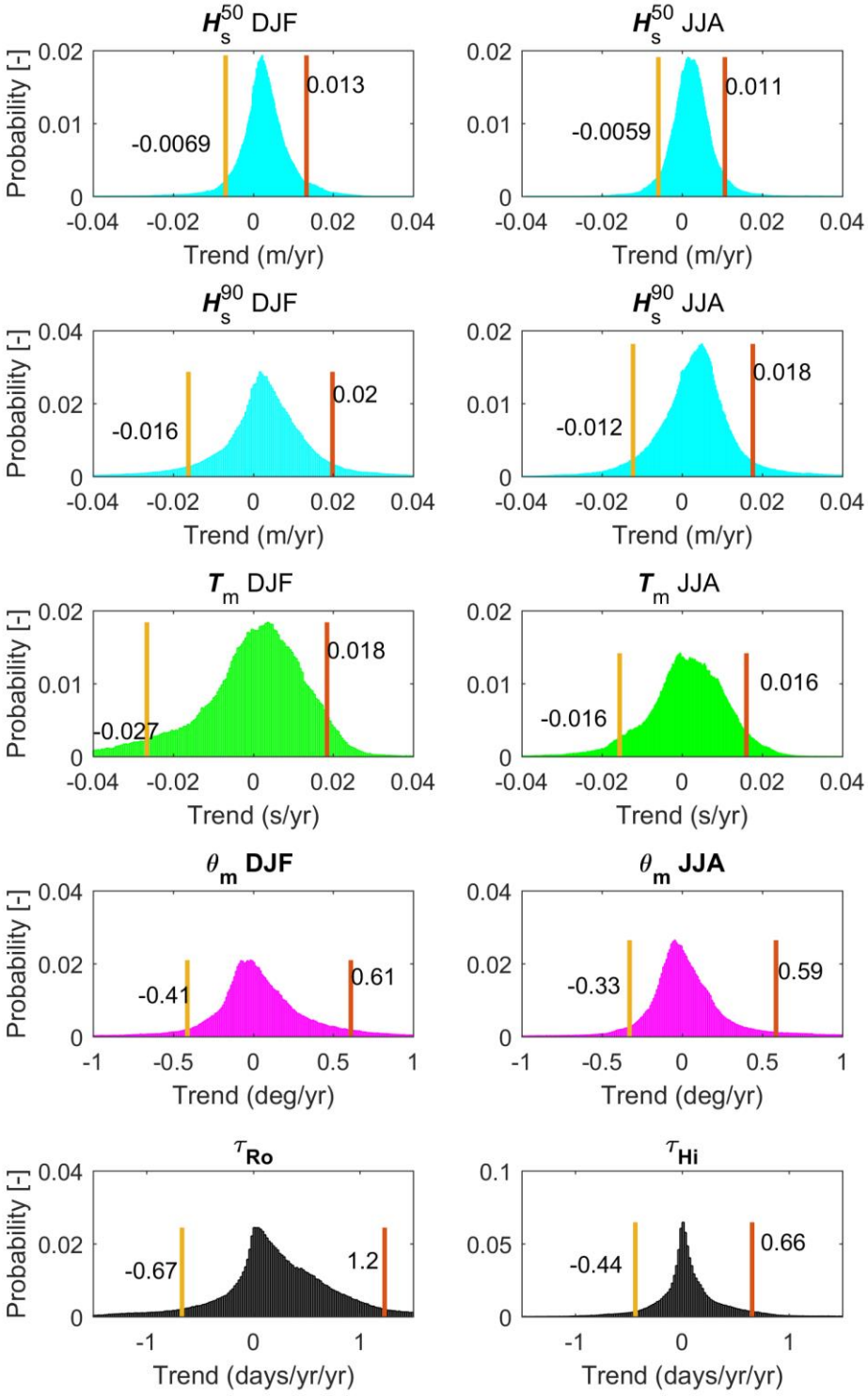

Supplementary Figure S6. Histograms showing probability densities of trends computed over the 35-year period 1980-2014 at all grid cells across all 7 ensemble members for each of the variables analyzed in this study. Vertical bars and values are the 5th and 95th percentiles of the complete sets.

4. Supplementary Notes 4: Influence of time-series duration on H_s trends

The sensitivity of trend values to the duration or time-slice of the record were analyzed by computing trends over three time-periods all ending in 2014 but starting in 1995, 1985, or 1980. The end date was selected based on overlapping availability of data for the majority of the contributed data products. The start dates are commensurate with the post step change of the CFSR driven products (1995) and approximate start date of the ESA-CCI altimeter data product, the start date of the IMOS altimeter reference data (1985) and start date of the 36-year time period of the ensemble (1980). All wave state products were gridded to a common 2x2 degree grid, trends calculated on each grid cell using each of the time-periods and averaged to produce the summary in Supplementary Table S3. Figure 1 in the main text illustrates the distributions via 'violin plots' and the difference in global medians (as opposed to means as presented in Supplementary Table S3) of each product and time slice. It is seen that the variance and range in trends associated with the shorter 21-year long record are in many cases more than twice that of the 36-year long record and sometimes differ in sign (direction). It is generally accepted that a minimum of 30 years is required to eliminate sampling on individual sections of natural atmosphere-ocean cycles and obtain robust representations of the climate[SM34,35]. The sensitivity test and results presented in Supplementary Table S3A and Figure 1 clearly show the sensitivity of this dataset to the length of the time-series, thus supporting the need to exclude shorter duration datasets (see Methods, Sections 3 and 4).

Supplementary Table S3A. Global average and standard deviation of H_s^{50} trends (cm/yr) computed at individual grid cells for three durations: 1995-2014, 1985-2014, and 1980-2014.

Product	Dec-Feb (DJF)			June-Aug (JJA)		
	1995-2014	1985-2014	1980-2014	1995-2014	1985-2014	1980-2014
ECMWF-ERA5	-0.30±0.89	0.29±0.45	0.42±0.41	-0.05±0.71	0.32±0.42	0.43±0.36
ECMWF-ERAI	-0.17±0.89	0.14±0.52	0.23±0.49	0.09±0.73	0.31±0.45	0.36±0.40
ECMWF-ERA5H	0.19±0.95	0.27±0.45	0.31±0.40	0.27±0.81	0.17±0.45	0.17±0.35
KU-JRA55	-0.24±1.11	-0.08±0.75	0.03±0.67	0.03±1.21	0.02±0.67	0.05±0.55
IORAS-MERRA2	-0.02±0.95	0.27±0.48	0.34±0.42	0.03±0.84	0.31±0.48	0.38±0.41
NOC-ERAI	0.14±1.00	0.19±0.54	0.25±0.47	0.32±0.93	0.08±0.47	0.10±0.38
IHC-GOW1.0	0.07±1.24	0.45±0.84	0.59±0.87	0.32±1.34	0.32±0.75	0.45±0.67
IHC-GOW2.0	0.62±1.33	-0.33±0.52	-0.35±0.52	0.74±1.07	-0.15±0.49	-0.28±0.48
CSIRO-CAWCR	0.68±1.36	-0.32±0.51	-0.35±0.50	0.76±1.06	-0.21±0.51	-0.31±0.51
IFREMER-CFSR	-0.34±1.07	-0.12±0.65	-0.09±0.58	-0.16±0.99	-0.16±0.67	-0.07±0.58
JRC-CFSR	0.55±1.31	-0.26±0.46	-0.32±0.47	0.63±1.01	-0.21±0.46	-0.29±0.44
JRC-ERAI	0.02±0.98	0.15±0.49	0.22±0.46	0.32±0.82	0.14±0.46	0.16±0.37
IORAS-VOS	-0.57±1.49	-0.09±1.01	0.11±0.90	-0.54±1.27	-0.43±0.76	-0.24±0.62
Altimeter 1 (IMOS)	-0.34±1.22	0.03±0.68	0.00±0.00	-0.34±1.06	0.09±0.65	0.00±0.00
Altimeter 2 (ESA-CCI)	0.49±1.10	0.00±0.00	0.00±0.00	0.55±0.99	0.00±0.00	0.00±0.00

Supplementary Table S3B. Global average and standard deviation of H_s^{90} trends (cm/yr) computed at individual grid cells for three durations: 1995-2014, 1985-2014, and 1980-2014.

Product	Dec-Feb (DJF)			June-Aug (JJA)		
	1995-2014	1985-2014	1980-2014	1995-2014	1985-2014	1980-2014
ECMWF-ERA5	-0.44±1.33	0.37±0.67	0.54±0.58	0.23±1.18	0.41±0.62	0.51±0.51
ECMWF-ERAI	-0.24±1.29	0.33±0.71	0.45±0.64	0.42±1.14	0.46±0.66	0.51±0.56
ECMWF-ERA5H	0.07±1.42	0.29±0.70	0.37±0.62	0.57±1.30	0.24±0.65	0.23±0.50
KU-JRA55	-0.41±1.61	-0.37±1.31	-0.08±1.10	0.19±1.73	-0.07±1.01	-0.03±0.82
IORAS-MERRA2	-0.10±1.38	0.31±0.80	0.42±0.66	0.13±1.27	0.42±0.75	0.51±0.60
NOC-ERAI	-0.03±1.45	0.18±0.84	0.27±0.69	0.52±1.36	0.10±0.71	0.11±0.57
IHC-GOW1.0	0.07±1.63	0.57±1.30	0.75±1.29	0.40±1.69	0.44±1.24	0.64±1.11
IHC-GOW2.0	0.77±1.87	-0.58±0.86	-0.63±0.83	1.09±1.45	-0.25±0.76	-0.46±0.71
CSIRO-CAWCR	0.85±1.87	-0.54±0.83	-0.60±0.82	1.13±1.42	-0.31±0.77	-0.48±0.74
IFREMER-CFSR	-0.35±1.44	-0.18±0.94	-0.15±0.83	-0.00±1.44	-0.22±1.01	-0.09±0.79
JRC-CFSR	0.66±1.84	-0.46±0.83	-0.53±0.80	0.92±1.43	-0.33±0.74	-0.44±0.67
JRC-ERAI	-0.14±1.41	0.14±0.77	0.24±0.67	0.54±1.25	0.17±0.69	0.20±0.56
IORAS-VOS	-0.89±2.16	-0.63±1.70	-0.36±1.33	-0.71±1.73	-0.80±1.22	-0.55±0.98
Altimeter 1 (IMOS)	-0.61±1.70	0.12±1.14	0.00±0.00	-0.51±1.59	0.40±1.17	0.00±0.00
Altimeter 2 (ESA-CCI)	0.32±1.60	0.00±0.00	0.00±0.00	0.77±1.46	0.00±0.00	0.00±0.00

5. Supplementary Notes 5: Influence of using alternative robustness measures

Ensemble mean trends and percent of areas within major global ocean regions experiencing robust signals of change were calculated using two measures of robustness[SM36]. Here, region and global mean trends are presented using the alternate criteria whereby robustness is assigned if more than 50% of the models (4 out of 7) exhibit significant trends ($pval < 0.05$) and at least 80% of those (> 3) agree on the sign of change[37]. Supplementary Table S4 and Supplementary Figures S7-9 are comparable to Table 2 and Figures 3-5 in the main text.

The results presented in the main text considers ensemble trends robust when the multi-member ensemble mean is greater than the inter-member standard deviation[38]

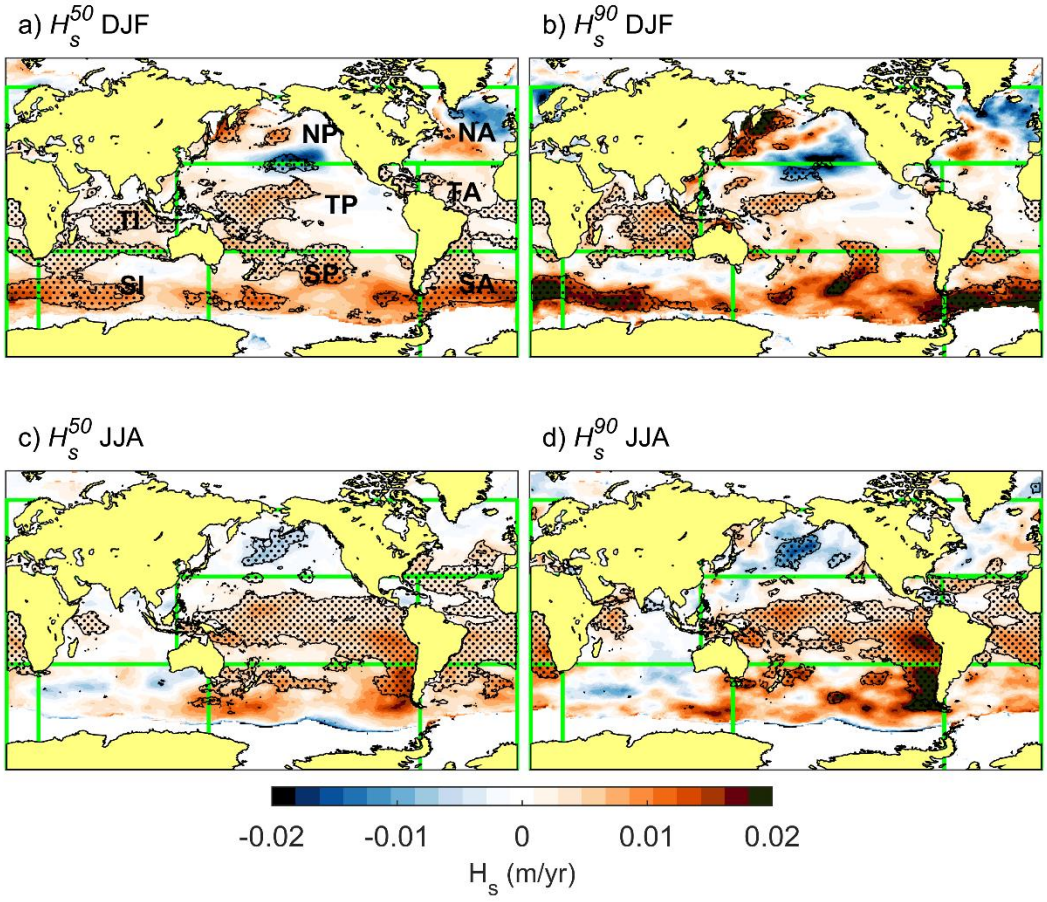

Supplementary Figure S7. Same as Figure 4 but using the robustness criteria that more than half of the models (4 out of 7) show significant trends and at least 80% of those (3 or more) agree on the sign of change.

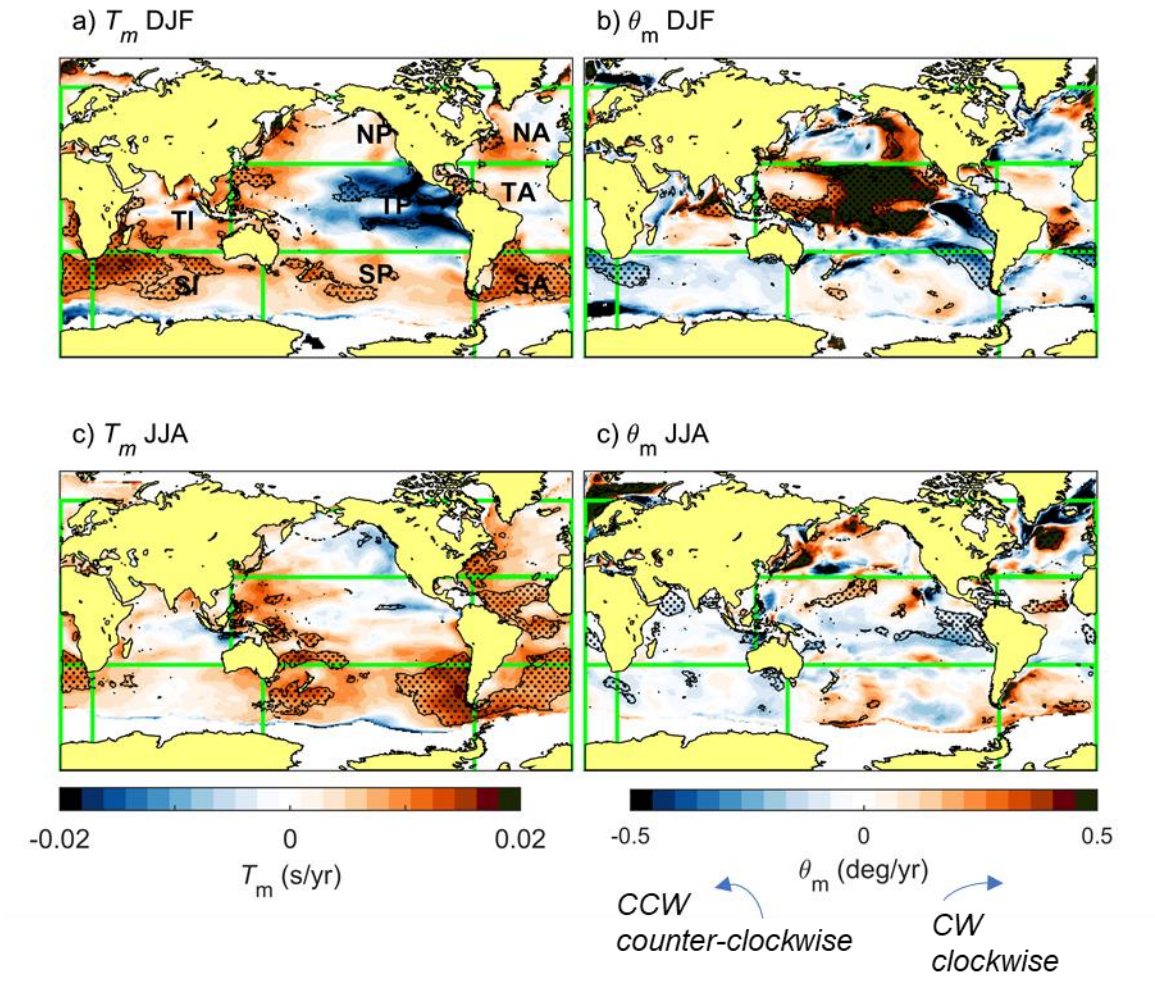

Supplementary Figure S8. Same as Figure 5 but using the robustness criteria that more than half of the models (4 out of 7) show significant trends and at least 80% of those (3 or more) agree on the sign of change.

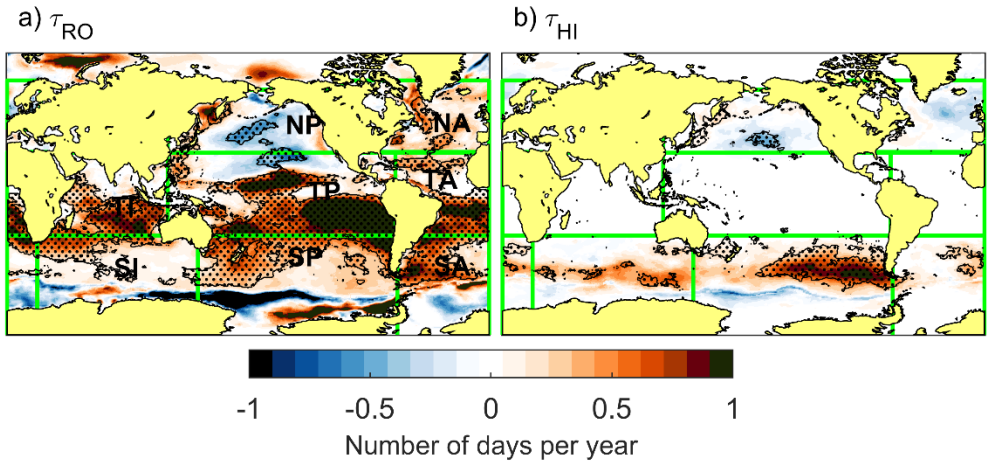

Supplementary Figure S9. Same as Figure 6 but using the robustness criteria that more than half of the models (4 out of 7) show significant trends and at least 80% of those (3 or more) agree on the sign of change.

Supplementary Table S4. Ensemble mean trends (cm/yr) and percent area experiencing robust signals of H_s change for of the DJF season using the robustness measure requirement that >50% of the models (4 out of 7) exhibit significant trends (ρ_{val} < 0.05) and at least 80% of those (> 3) agree on the direction of change.

	H_s^{50} DJF				H_s^{90} DJF			
Regions	positive trend cm/yr		negative trend cm/yr		positive trend cm/yr		negative trend cm/yr	
	% area	mean	% area	mean	% area	mean	% area	mean
NP	11	0.85±0.27	4	-1.46±0.24	15	1.59±0.57	1	-2.21±0.09
NA	1	0.85±0.15	2	-1.04±0.28	0	1.27±0.07	1	-1.61±0.45
TP	25	0.50±0.14	2	-0.80±0.31	12	0.72±0.21	2	-1.23±0.44
TA	32	0.43±0.14	1	-0.82±0.34	22	0.62±0.21	1	-1.24±0.47
TI	43	0.40±0.12	0	-0.12±0.07	50	0.62±0.18	0	-0.23±0.07
SP	22	0.76±0.28	0	-0.06±0.00	10	1.33±0.46	0	NaN
SA	29	0.79±0.32	0	-0.06±0.00	19	1.34±0.52	0	NaN
SI	32	0.69±0.24	0	NaN	23	1.20±0.52	0	NaN
Globe	***23***	***0.61±0.31***	***1***	***-1.04±0.43***	***16***	***1.00±0.56***	***1***	***-1.35±0.53***

NP: North Pacific. NA: North Atlantic. SP: South Pacific. SA: South Atlantic. TA: Tropical Atlantic. TP: Tropical Pacific. TI: Tropical Indian Ocean. SI: South Indian Ocean

Supplementary Table S5. Ensemble mean trends (cm/yr) and percent area experiencing robust signals of H_s change for of the JJA season using the robustness measure requirement that >50% of the models (4 out of 7) exhibit significant trends (ρ_{val} < 0.05) and at least 80% of those (> 3) agree on the direction of change.

	H_s^{50} JJA				H_s^{90} JJA			
Regions	positive trend cm/yr)		negative trend cm/yr)		positive trend cm/yr)		negative trend cm/yr)	
	% area	mean	% area	mean	% area	Mean	% area	mean
NP	2	0.25±0.07	17	-0.52±0.13	3	0.58±0.09	16	-0.98±0.30
NA	22	0.37±0.12	0	-0.24±0.06	6	0.57±0.22	1	-0.58±0.13
TP	57	0.53±0.21	0	-0.25±0.08	51	0.74±0.34	1	-0.51±0.14
TA	50	0.49±0.20	0	-0.25±0.07	46	0.70±0.31	1	-0.44±0.14
TI	8	0.33±0.07	0	-0.19±0.05	14	0.56±0.15	3	-0.44±0.13
SP	16	0.87±0.31	0	-1.01±0.16	14	1.53±0.42	0	NaN
SA	12	0.78±0.29	0	-0.75±0.11	7	1.46±0.42	0	NaN
SI	2	0.85±0.30	0	-0.73±0.07	1	1.29±0.17	0	NaN
Globe	***23***	***0.54±0.25***	***1***	***-0.49±0.16***	***20***	***0.80±0.42***	***2***	***-0.80±0.35***

Supplementary Table S6. Ensemble mean trends and percent area experiencing robust signals of change for T_m (sec/yr) and D_m (deg/yr) during the DJF season using the robustness measure requirement that >50% of the models (4 out of 7) exhibit significant trends (ρ_{val} < 0.05) and at least 80% of those (> 3) agree on the direction of change.

	T_m DJF				θ_m DJF			
Region	positive trend (s/yr)		negative trend (s/yr)		CW trend (°/yr)		CCW trend (°/yr)	
	% area	mean	% area	mean	% area	mean	% area	mean
NP	2	0.012±0.005	0	NaN	9	0.40±0.14	0	-0.28±0.23
NA	2	0.011±0.002	0	NaN	0	0.68±0.33	0	-0.88±0.32
TP	1	0.009±0.001	10	-0.017±0.004	34	0.54±0.23	8	-0.42±0.21
TA	3	0.010±0.003	6	-0.017±0.004	22	0.52±0.23	6	-0.40±0.21
TI	8	0.010±0.003	0	NaN	7	0.32±0.14	2	-0.19±0.08
SP	5	0.009±0.001	0	NaN	1	0.17±0.04	6	-0.27±0.14
SA	14	0.011±0.002	0	NaN	1	0.18±0.11	7	-0.25±0.12
SI	16	0.011±0.003	0	NaN	0	2.04±0.00	6	-0.19±0.04
Globe	***7***	***0.011±0.003***	***2***	***-0.017±0.004***	***9***	***0.51±0.27***	***5***	***-0.32±0.18***

Supplementary Table S7. Ensemble mean trends and percent area experiencing robust signals of change for T_m (sec/yr) and θ_m (deg/yr) during the JJA season using the robustness measure requirement that >50% of the models (4 out of 7) exhibit significant trends (ρ_{val} < 0.05) and at least 80% of those (> 3) agree on the direction of change.

	T_m JJA				θ_m JJA			
Region	positive trend (s/yr)		negative trend (s/yr)		CW trend (°/yr)		CCW trend (°/yr)	
	% area	mean	% area	mean	% area	mean	% area	mean
NP	1	0.011±0.002	0	-0.005±0.000	4	0.49±0.16	1	-0.39±0.19
NA	6	0.010±0.002	0	NaN	7	0.58±0.26	2	-0.50±0.30
TP	9	0.011±0.002	0	-0.014±0.005	5	0.19±0.13	10	-0.16±0.09
TA	11	0.010±0.002	0	-0.014±0.004	4	0.20±0.12	10	-0.13±0.08
TI	1	0.007±0.001	1	-0.013±0.002	1	0.15±0.07	12	-0.11±0.06
SP	4	0.012±0.003	0	NaN	1	0.24±0.03	0	-0.22±0.01
SA	7	0.010±0.002	0	NaN	1	0.27±0.11	2	-0.15±0.02
SI	0	0.006±0.000	0	NaN	0	NaN	4	-0.14±0.02
Globe	***14***	***0.008±0.002***	***0***	***-0.007±0.003***	***3***	***0.40±0.40***	***5***	***-0.15±0.12***

Supplementary Table S8. Ensemble mean trends (days/yr·yr) and percent area experiencing robust signals of change in the number of rough (τ_{RO}) and high (τ_{HI}) wave days using the robustness measure requirement that >50% of the models (4 out of 7) exhibit significant trends (ρ_{val} < 0.05) and at least 80% of those (> 3) agree on the direction of change.

	τ_{RO}				τ_{HI}			
Region	positive trend (days/yr·yr)		negative trend (days/yr·yr)		positive trend (days/yr·yr)		negative trend (days/yr·yr)	
	% area	mean	% area	mean	% area	Mean	% area	mean
NP	6	0.41±0.20	10	-0.52±0.08	6	0.13±0.05	6	-0.39±0.07
NA	14	0.43±0.13	1	-0.35±0.09	1	0.08±0.03	0	-0.04±0.02
TP	52	0.83±0.41	3	-0.52±0.12	0	0.04±0.01	0	-0.05±0.02
TA	54	0.73±0.37	2	-0.52±0.12	0	0.04±0.01	0	-0.05±0.03
TI	52	0.58±0.22	0	-0.04±0.03	0	0.03±0.00	0	NaN
SP	33	0.53±0.22	0	NaN	23	0.53±0.28	0	NaN
SA	30	0.52±0.23	0	NaN	14	0.47±0.26	0	-0.06±0.01
SI	23	0.42±0.21	0	NaN	7	0.42±0.15	0	-0.06±0.01
Globe	***31***	***0.64±0.34***	***1***	***-0.51±0.11***	***6***	***0.44±0.27***	***0***	***-0.32±0.15***

6. Supplementary Notes 6: Sensitivity of trends to moving averages

Prior to fitting trend lines to each grid cell time-series, a 3-year moving average was applied[SM39,40] to reduce natural (atmospheric) decadal and multidecadal variability (such as PDO and ENSO, which have cycles of ~10 years and ~2-7 years, respectively). The influence of applying a moving mean was evaluated by computing trend statistics using a 3-year, 5-year, or no moving mean at each grid cell and plotting histograms to evaluate the influence on the overall global trends. Supplementary Figure S10A shows resulting histograms for DJF H_s^{90} of each product and indicates that the moving means have little influence on the overall result. Whence considering only those grid cells for which statistically significant trends (p-value<0.05) exist, it is seen that the patterns of overall negative or positive trends are similar independent of the number of years used for a moving average, but that the number of grid cells with significant trends increases with the length of the moving average (Supplementary Fig. S10B).

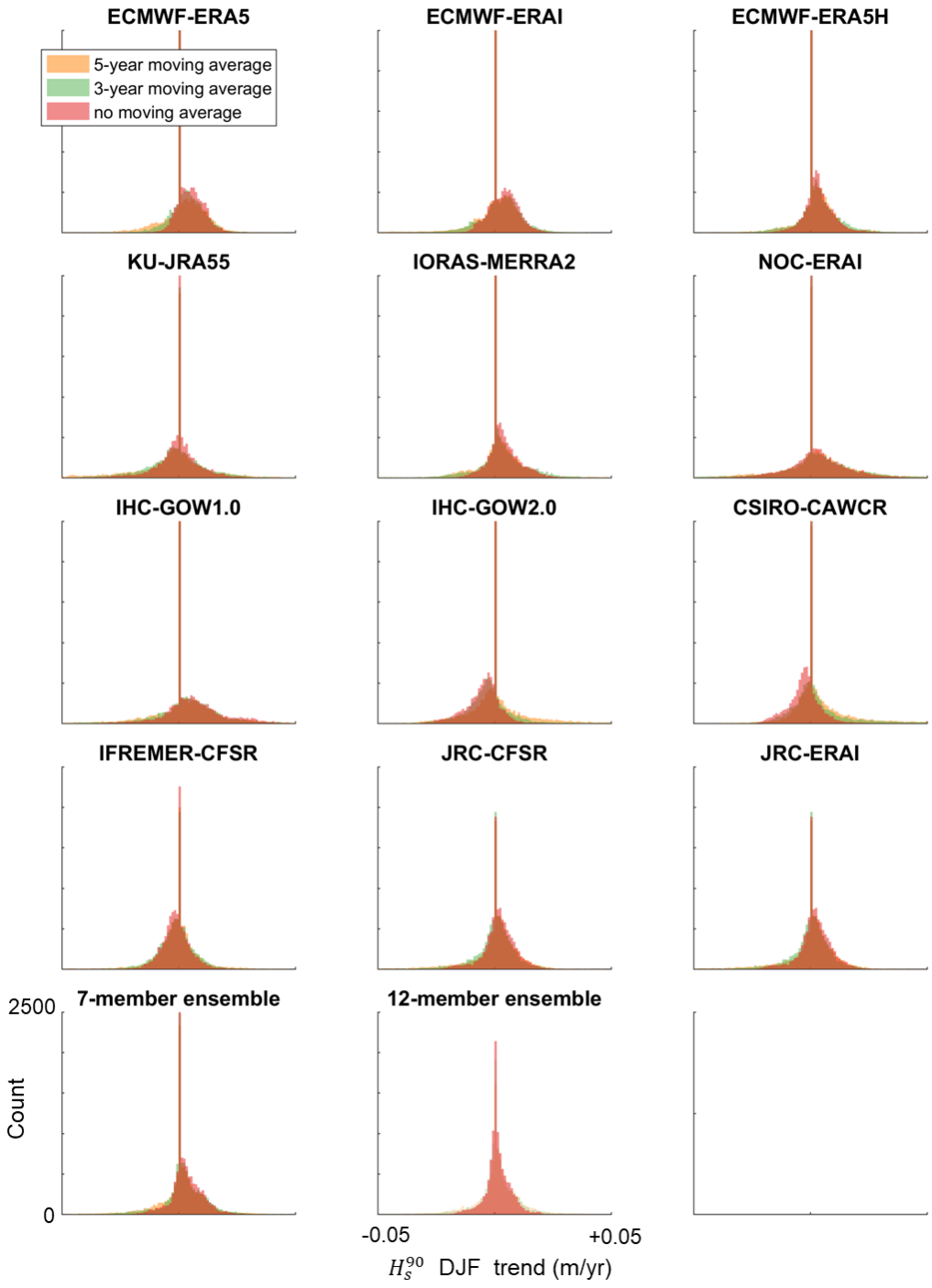

Supplementary Figure S10A. Sensitivity of trends (m/yr) in H_s^{90} DJF wave heights using 5-year, 3-year, or no moving average across all time-points. Histograms for all grid cells across the globe for each model and 7-member and 12-member ensemble are shown.

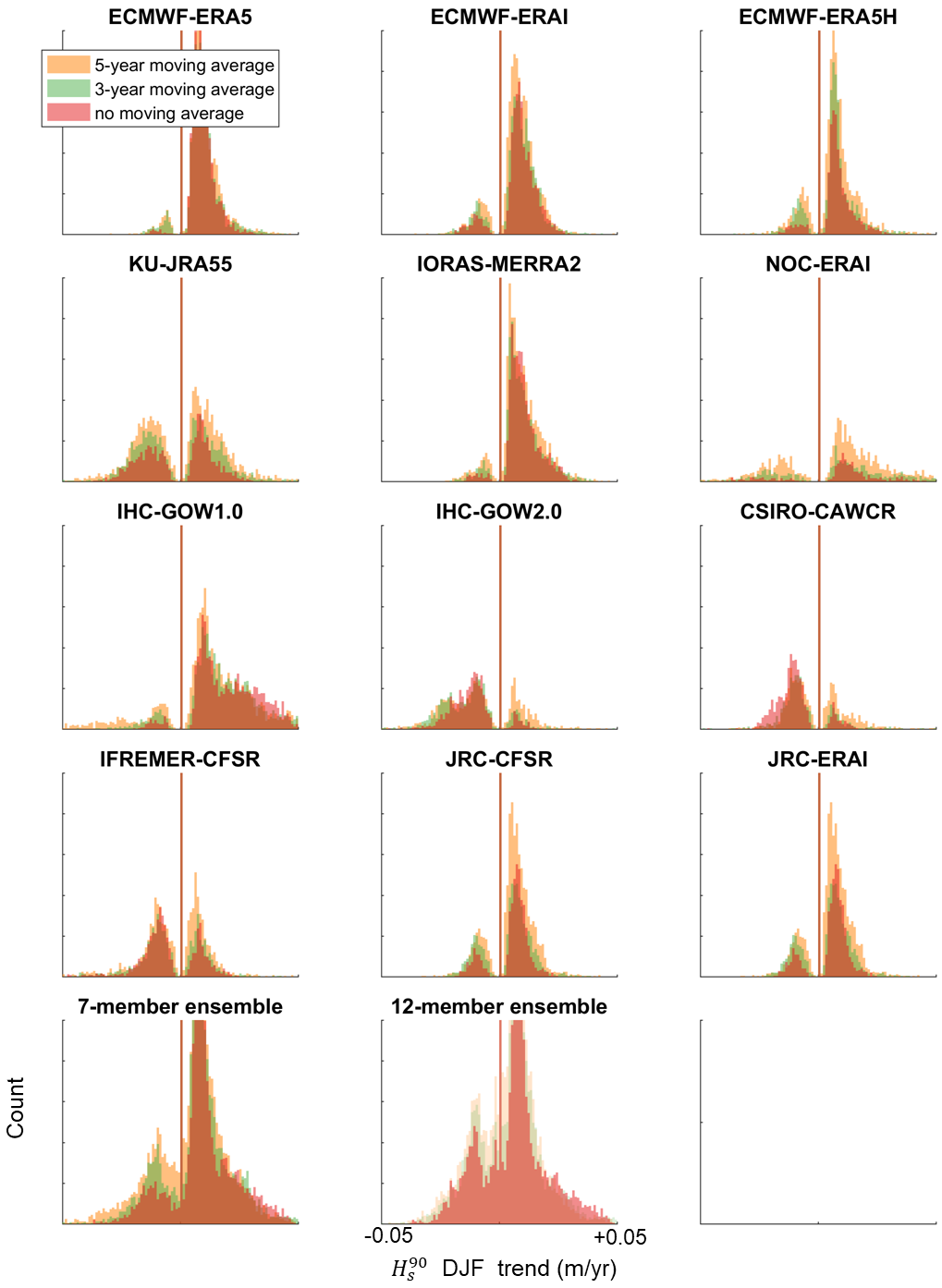

Supplementary Figure S10B. Same as in Supplementary Figure S10A but only those points for which trend values were statistically significant (p-values<0.05) are shown.

Supplementary References

1 Dee, D. P. *et al.* The ERA-Interim reanalysis: configuration and performance of the data assimilation system. *Quarterly Journal of the Royal Meteorological Society* **137**, 553-597 (2011). https://doi.org:https://doi.org/10.1002/qj.828

2 Stopa, J. E. & Cheung, K. F. Intercomparison of wind and wave data from the ECMWF Reanalysis Interim and the NCEP Climate Forecast System Reanalysis. *Ocean Modelling* **75**, 65-83 (2014). https://doi.org:10.1016/j.ocemod.2013.12.006

3 Aarnes, O. J., Abdalla, S., Bidlot, J.-R. & Breivik, Ø. Marine Wind and Wave Height Trends at Different ERA-Interim Forecast Ranges. *Journal of Climate* **28**, 819-837 (2015). https://doi.org:10.1175/jcli-d-14-00470.1

4 Hersbach, H. *et al.* The ERA5 global reanalysis. *Quarterly Journal of the Royal Meteorological Society* **146**, 1999-2049 (2020). https://doi.org:https://doi.org/10.1002/qj.3803

5 Bidlot, J., Lemos, G., Semedo, S. in *2nd International Workshop on Waves, Storm Surges, and Coastal Hazards* (2019).

6 ECMWF. Official IFS Documentation CY47R1. In chap. PART VII: ECMWF wave model. Reading, UK: ECMWF. https://www.ecmwf.int/en/publications/ifs-documentation. (2020).

7 Mori, N., Shimura, T., Kamahori, H. & Chawla, A. in *Coastal Dynamics.* (eds T. Aagaard, R Deigaard, & D. Fhurman) 117-124.

8 Shimura, T., Mori, N. & Hemer, M. A. Variability and future decreases in winter wave heights in the Western North Pacific. *Geophysical Research Letters* **43**, 2716-2722 (2016). https://doi.org:https://doi.org/10.1002/2016GL067924

9 Sharmar, V., Margarita, M. & Gulev, S. *Global wind wave climate variability based on MERRA-2 wind wave hindcast*. (2018).

10 Bricheno, L. M. & Wolf, J. Future Wave Conditions of Europe, in Response to High-End Climate Change Scenarios. *Journal of Geophysical Research: Oceans* **123**, 8762-8791 (2018). https://doi.org:https://doi.org/10.1029/2018JC013866

11 Reguero, B. G., Menéndez, M., Méndez, F. J., Mínguez, R. & Losada, I. J. A Global Ocean Wave (GOW) calibrated reanalysis from 1948 onwards. *Coastal Engineering* **65**, 38-55 (2012). https://doi.org:https://doi.org/10.1016/j.coastaleng.2012.03.003

12 Perez, J., Menendez, M. & Losada, I. J. GOW2: A global wave hindcast for coastal applications. *Coastal Engineering* **124**, 1-11 (2017). https://doi.org:https://doi.org/10.1016/j.coastaleng.2017.03.005

13 Durrant, T. H., M; Trenham, C; Greenslade, D. (ed CAWCR) (2013).

14 Smith, G. A. *et al.* Global wave hindcast with Australian and Pacific Island Focus: From past to present. *Geoscience Data Journal* **n/a** (2020). https://doi.org:https://doi.org/10.1002/gdj3.104

15 Stopa, J. E., Ardhuin, F., Stutzmann, E. & Lecocq, T. Sea State Trends and Variability: Consistency Between Models, Altimeters, Buoys, and Seismic Data (1979–2016). *Journal of Geophysical Research: Oceans* **124**, 3923-3940 (2019). https://doi.org:10.1029/2018JC014607

16 Ardhuin, F. *et al.* Semiempirical Dissipation Source Functions for Ocean Waves. Part I: Definition, Calibration, and Validation. *Journal of Physical Oceanography* **40**, 1917-1941 (2010). https://doi.org:10.1175/2010jpo4324.1

17 Hasselmann, S. & K., H. Computations and parameterizations of the nonlinear energy transfer in a gravity-wave spectrum. Part I: A new method for efficient computations of the exact nonlinear transfer integral. . *J. Phys. Oceanogr* **15**, 8 (1985).

18 Stopa, J. E., Ardhuin, F., Babanin, A. & Zieger, S. Comparison and validation of physical wave parameterizations in spectral wave models. *Ocean Modelling* **103**, 2-17 (2016). https://doi.org:10.1016/j.ocemod.2015.09.003

19 Saha, S. & Coauthors, a. The NCEP Climate Forecast System Version 2 *Journal of Climate* **27**, 2185–2208 (2014). https://doi.org:http://dx.doi.org/10.1175/JCLI-D-12-00823.1

20 Saha, S. *et al.* The NCEP Climate Forecast System Reanalysis. *Bulletin of the American Meteorological Society* **91**, 1015-1058 (2010). https://doi.org:10.1175/2010bams3001.1

21 Queffeulou, P. & Croizé-fillon, D. Global Altimeter SWH data set. 8 (IFREMER, 2012).

22 Stopa, J. E. Wind forcing calibration and wave hindcast comparison using multiple reanalysis and merged satellite wind datasets. *Ocean Modelling* **127**, 55-69 (2018). https://doi.org:10.1016/j.ocemod.2018.04.008

23 Rascle, N. & Ardhuin, F. A global wave parameter database for geophysical applications. Part 2: Model validation with improved source term parameterization. *Ocean Modelling* **70**, 174-188 (2013). https://doi.org:https://doi.org/10.1016/j.ocemod.2012.12.001

24 Chawla, A., Spindler, D. M. & Tolman, H. L. Validation of a thirty year wave hindcast using the Climate Forecast System Reanalysis winds. *Ocean Modelling* **70**, 189-206 (2013). https://doi.org:https://doi.org/10.1016/j.ocemod.2012.07.005

25 Mentaschi, L., Vousdoukas, M. I., Voukouvalas, E., Dosio, A. & Feyen, L. Global changes of extreme coastal wave energy fluxes triggered by intensified teleconnection patterns. *Geophysical Research Letters* **44**, 2416-2426 (2017). https://doi.org:https://doi.org/10.1002/2016GL072488

26 Freeman, E. *et al.* ICOADS Release 3.0: a major update to the historical marine climate record. *International Journal of Climatology* **37**, 2211-2232 (2017). https://doi.org:https://doi.org/10.1002/joc.4775

27 Gulev, S. K., Grigorieva, V., Sterl, A. & Woolf, D. Assessment of the reliability of wave observations from voluntary observing ships: Insights from the validation of a global wind wave climatology based on voluntary observing ship data. *Journal of Geophysical Research: Oceans* **108** (2003). https://doi.org:https://doi.org/10.1029/2002JC001437

28 Grigorieva, V. G., Gulev, S. K. & Gavrikov, A. V. Global historical archive of wind waves based on Voluntary Observing Ship data. *Oceanology* **57**, 229-231 (2017). https://doi.org:10.1134/S0001437017020060

29 Gulev, S. K. & Grigorieva, V. Last Century changes in ocean wind wave height from global visual wave data. *Geophysical Research Letters* **31** (2004). https://doi.org:10.1029/2004GL021040

30 Gulev, S. K. & Grigorieva, V. Variability of the winter wind waves and swell in the north Atlantic and North Pacific as Revealed by the Voluntary Observing Ship Data. *Journal of Climate* **19**, 19 (2006).

31 Ribal, A. & Young, I. R. 33 years of globally calibrated wave height and wind speed data based on altimeter observations. *Sci Data* **6**, 77 (2019). https://doi.org:10.1038/s41597-019-0083-9

32 Dodet, G. *et al.* The Sea State CCI dataset v1: towards a sea state climate data record based on satellite observations. *Earth Syst. Sci. Data* **12**, 1929-1951 (2020). https://doi.org:10.5194/essd-12-1929-2020

33 Willmott, C. J. *et al.* Statistics for the evaluation and comparison of models. *Journal of Geophysical Research* **90**, 8995 (1985). https://doi.org:10.1029/JC090iC05p08995

34 Chen, Z. & Grasby, S. E. Impact of decadal and century-scale oscillations on hydroclimate trend analyses. *Journal of Hydrology* **365**, 122-133 (2009). https://doi.org:10.1016/j.jhydrol.2008.11.031

35 Cubasch, U. *et al.* in *Climate Change 2013: The Physical Science Basis. Contribution of Working Group I to the Fifth Assessment Report of the Intergovernmental Panel on Climate Change.* (eds T.F. Stocker, D. Qin, G.-K. Plattner, M. Tignor, S.K. Allen, & A. Nauels J. Boschung, Y. Xia, V. Bex and P.M. Midgley (eds.)]) Ch. 1, 119-158 (Cambridge University Press, 2013).

36 Collins, M. e. a. In Climate Change 2013: The Physical Science Basis (eds Stocker, T. F. et al.) (Cambridge Univ. Press, 2013).

37 Tebaldi, C., Arblaster, J. M. & Knutti, R. Mapping model agreement on future climate projections. *Geophysical Research Letters* **38** (2011). https://doi.org:10.1029/2011GL049863

38 Hemer, M. A. & Trenham, C. E. Evaluation of a CMIP5 derived dynamical global wind wave climate model ensemble. *Ocean Modelling* **103**, 190-203 (2016). https://doi.org:10.1016/j.ocemod.2015.10.009

39 Hegerl, G. C. *et al.* Causes of climate change over the historical record. *Environmental Research Letters* **14** (2019). https://doi.org:10.1088/1748-9326/ab4557

40 Wu, T., Hu, A., Gao, F., Zhang, J. & Meehl, G. A. New insights into natural variability and anthropogenic forcing of global/regional climate evolution. *npj Climate and Atmospheric Science* **2** (2019). https://doi.org:10.1038/s41612-019-0075-7